LEBANESE AMERICAN UNIVERSITY

A 2x2 Space-Time Code for Non-Coherent Ultra WideBand (UWB) Communication Systems with M-PPM and Energy Detection

By

Ali H. El Amine

A thesis
submitted in partial fulfillment of the requirements
for the degree of Master of Science in Engineering

School of Engineering

June 2016

Lebanese American University

School of Engineering, Byblos Campus

THESIS APPROVAL FORM

Student Name: ALI EL AMINE I.D. #: 200803058

Thesis Title : A 2x2 Space-Time Code for Non-Coherent UltraWideband (UWB) Communication Systems with M-PPM and Energy Detection

Program: Ms. in Computer Engineering

Department: ELectrical and Computer Engineering

School: Engineering

The undersigned certify that they have examined the final electronic copy of this thesis and approved it in Partial Fulfillment of the requirements for the degree of:

Ms. in Computer Engineering in the major of Computer and Communication Engineering

Thesis Advisor's Name Chadi Abou-Rjeily Signat [redacted] 01/06/2016

Committee Member's Name Wissam FAWAZ Signature [redacted] ate 01/06/2016

Committee Member's Name Samer Sa.b S [redacted] 01/06/2016

LAU
الجامعة اللبنانية الأميركية
Lebanese American University

THESIS COPYRIGHT RELEASE FORM

LEBANESE AMERICAN UNIVERSITY NON-EXCLUSIVE DISTRIBUTION LICENSE

By signing and submitting this license, you (the author(s) or copyright owner) grants to Lebanese American University (LAU) the non-exclusive right to reproduce, translate (as defined below), and/or distribute your submission (including the abstract) worldwide in print and electronic format and in any medium, including but not limited to audio or video. You agree that LAU may, without changing the content, translate the submission to any medium or format for the purpose of preservation. You also agree that LAU may keep more than one copy of this submission for purposes of security, backup and preservation. You represent that the submission is your original work, and that you have the right to grant the rights contained in this license. You also represent that your submission does not, to the best of your knowledge, infringe upon anyone's copyright. If the submission contains material for which you do not hold copyright, you represent that you have obtained the unrestricted permission of the copyright owner to grant LAU the rights required by this license, and that such third-party owned material is clearly identified and acknowledged within the text or content of the submission. IF THE SUBMISSION IS BASED UPON WORK THAT HAS BEEN SPONSORED OR SUPPORTED BY AN AGENCY OR ORGANIZATION OTHER THAN LAU, YOU REPRESENT THAT YOU HAVE FULFILLED ANY RIGHT OF REVIEW OR OTHER OBLIGATIONS REQUIRED BY SUCH CONTRACT OR AGREEMENT. LAU will clearly identify your name(s) as the author(s) or owner(s) of the submission, and will not make any alteration, other than as allowed by this license, to your submission.

Name: [redacted]

Signatur[redacted]

Date: 01/06/2016

LAU
الجامعة اللبنانية الأميركية
Lebanese American University

PLAGIARISM POLICY COMPLIANCE STATEMENT

I certify that:

- I have read and understood LAU's Plagiarism Policy.
- I understand that failure to comply with this Policy can lead to academic and disciplinary actions against me.
- This work is substantially my own, and to the extent that any part of this work is not my own I have indicated that by acknowledging its sources.

Name: ALI H. EL AMINE

Signature [redacted]

Date: 01/06/2016

A 2x2 Space-Time Code for Non-Coherent Ultra WideBand (UWB) Communication Systems with M-PPM and Energy Detection

Ali H. El Amine

ABSTRACT

It is all about spectrum, the electromagnetic communication frequency spectrum characterizes the distribution of all the different wireless technologies approved by the Federal Communications Commission (FCC) and their emitted radiation power in a way that minimizes the interference between two or more wireless systems. All electronic communications compel a transmission medium to transmit the information from one location (transmitter) to another (receiver). In radio frequency (RF), the medium is free space. Today most of our electronic devices use the wireless channel for communication of either voice or data. In order to overcome interference between the numerous signals hovering in free space, each communication system should process its own allocated frequency band. As the request for higher capacity and faster services increases, new improved technologies have to find their room in the crowded spectrum. Ultra-wideband (UWB) technology provides a bright solution to the over populated RF spectrum by allowing new communication systems to coexist with the present radio with almost no interference.

In order to increase the capacity with UWB systems to achieve high data rates, the use of space-time coding (STC) with Multiple Input Multiple Output (MIMO) systems is considered. This can be realized by transmitting independently and simultaneously several symbols over different time intervals due to the antenna diversity introduced with MIMO systems.

In this work, we present a noncoherent space-time block code based on a coherent one discussed in the literature for M-PPM modulation associated with Impulse-Radio Ultra-Wideband (IR-UWB) systems where neither the receiver nor the transmitter has knowledge of the channel's parameters. The proposed scheme takes advantages of

the Multiple Input Multiple output (MIMO) system and achieves a full transmit diversity with two transmitters at the cost of a reduced coding rate while being shape preservative and totally real. The main advantage resides in a compelling adaptability to simple energy detection bypassing involved analog to digital conversion.

Keywords: IR-UWB, Wireless communication, Diversity Gain, Transmit diversity, MIMO systems, Code rate, M-PPM, Space-Time coding, Energy detection, Non-Coherent systems, Block-by-Block modulation, Shape preserving.

TABLE OF CONTENTS

List of Figures

List of Tables

List of Abbreviations

UWB	**U**ltra **W**ide**B**and
IR	**I**mpulse **R**adio
PG	**P**rocessing **G**ain
SISO	**S**ingle **I**nput **S**ingle **O**utput
MIMO	**M**ultiple **I**nput **M**ultiple **O**utput
MISO	**M**ultiple **I**nput **S**ingle **O**utput
SIMO	**S**ingle **I**nput **M**ultiple **O**utput
FCC	**F**ederal **C**ommunications **C**ommission
LOS	**L**ine **O**f **S**ight
NLOS	**N**o **L**ine **O**f **S**ight
CSI	**C**hannel **S**tate **I**nformation
MAI	**M**ultiple **A**ccess **I**nterference
QAM	**Q**uadrature **A**mplitude **M**odulation
PPM	**P**ulse **P**osition **M**odulation
PSK	**P**ahse **S**hift **K**eying
BPSK	**B**inary **P**hase **S**hift **k**eying
DPSK	**D**ifferential **P**hase **S**hift **k**eying
ADC	**A**nalog **D**igital **C**onverter
DSP	**D**igital **S**ignal **P**rocessing
BER	**B**it **E**rror **R**ate
SNR	**S**ignal to **N**oise **R**atio
MRC	**M**aximal **R**atio **C**ombiner
EGC	**E**qual **G**ain **C**ombiner
ST	**S**pace **T**ime
STC	**S**pace **T**ime **C**ode
STBC	**S**pace **T**ime **B**lock **C**ode
OSTBC	**O**rthogonal **S**pace **T**ime **B**lock **C**ode
DSTBC	**D**ifferential **S**pace **T**ime **B**lock **C**ode

Chapter 1

INTRODUCTION

1.1 Ultra-Wideband Systems (UWB)

1.1.1 What is UWB?

1.1.1.1 History and Background

Ultra-Wideband is an old technology that started with Guglielmo Marconi back in 1901 to transmit Morse code sequences over the Atlantic Ocean using pulse gap radio transmitters [1]. Around the year 1980, this technology was classified for military use applications mainly for radar systems because of its wideband nature that results in very accurate timing information [2]. However, due to the increase demand in data rates, capacity and as a result of new advanced microprocessors and fast switching in semiconductor technology, UWB surfaced its way out to be ready to be used for commercial applications. And in February 2002, the Federal Communications Commission (FCC) approved the "First Report and Order (R&O)" for allowing the use of commercial products adopting UWB technology under firm power emission limits [3].

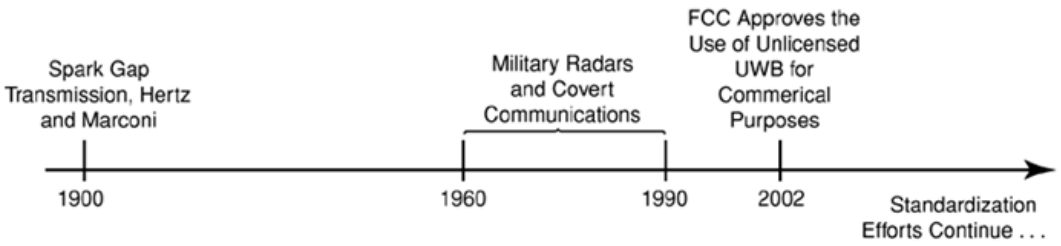

FIGURE 1.1: A brief history of UWB evolution

1.1.1.2 Concept

In traditional communication systems, the baseband sinusoidal information signal is modulated with a defined carrier frequency over the channel between the receiver and the transmitter resulting in a narrow band frequency and a power exceeding the channel noise making it exposed to detection and interruption. Figure 1.2 displays a narrowband signal in the time and frequency domains respectively.

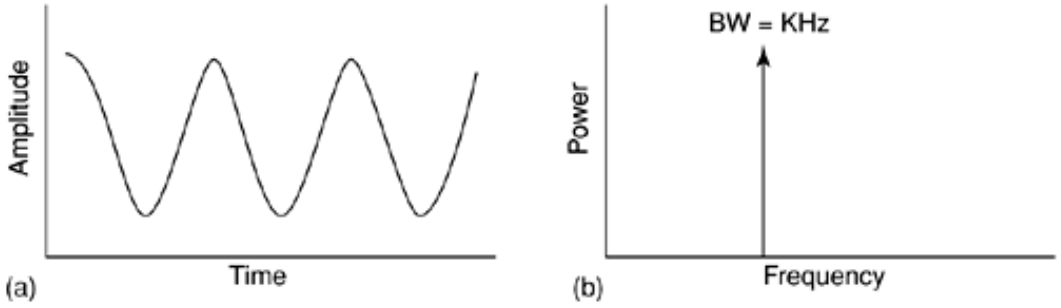

FIGURE 1.2: Narrowband signal in the time vs frequency domains

In contrast to the previous model, Ultra-Wideband communications are carrierless and use extremely narrow RF pulses (picoseconds to nanoseconds of duration) to communicate between transmitters and receivers; hence generating a very wide bandwidth. Such wide bandwidth is the result of the inverse relationship between time and frequency. With UWB, signals are compressed in time; hence resulting in a stretched frequency bandwidth as shown in figure 1.3.

The FCC has allocated the frequency band that UWB signals shall use for indoor communication systems ranging from 3.1 to 10.6 GHz with a bandwidth of at least 500

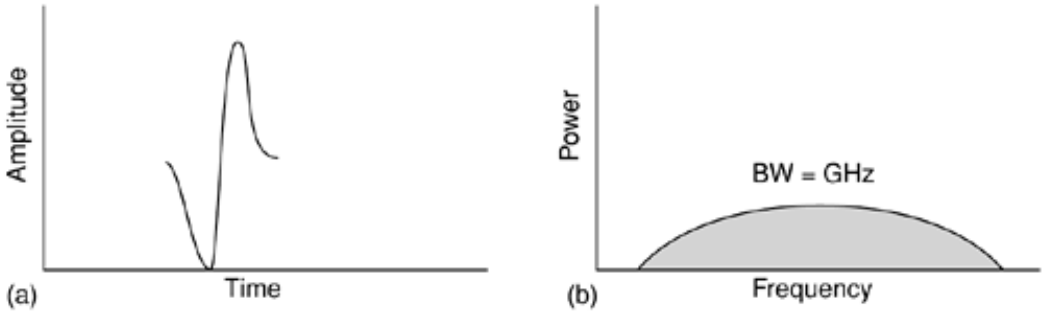

FIGURE 1.3: Wideband signal in the time vs frequency domains

MHz [3]. In order to prevail interference with other technologies employed in such spectrum, the FCC has limited the transmitted power of UWB signals to beneath the noise floor level which corresponds to -41.3 dBm.MHz^{-1} as shown in the figure 1.4.

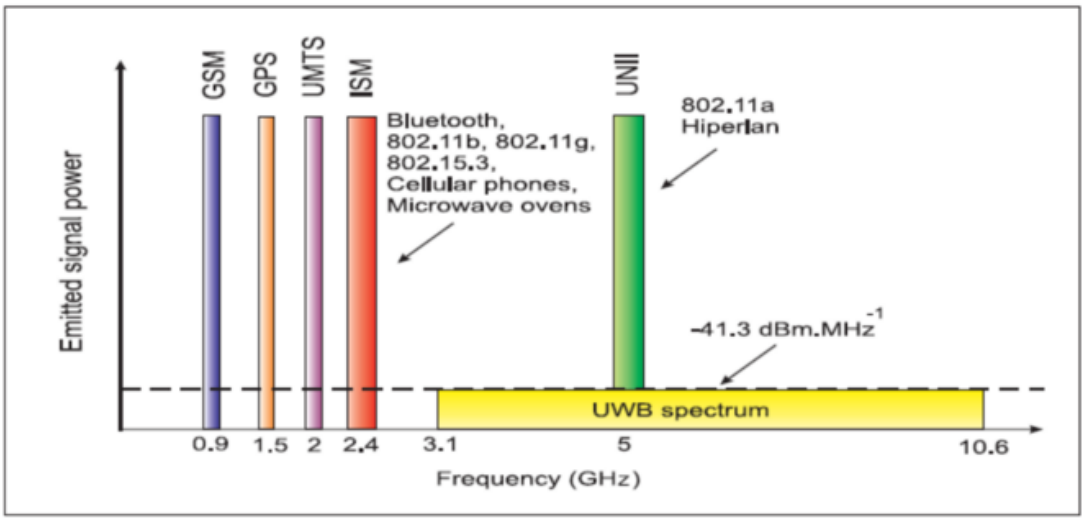

FIGURE 1.4: UWB signals' power below the noise floor level

1.1.2 Advantages

UWB technology holds many advantages over narrowband communication systems. We present the following major ones:

1.1.2.1 Ability to Share the Frequency Spectrum

As previously mentioned, UWB systems allocate a frequency bandwidth spectrum that range from 3.1 to 10.6 GHz; however, other narrowband services such as wideband, CDMA and Bluetooth also exist in the same bandwidth which will cause interference if not controlled. In order to minimize this interference, the FCC has restricted the power of using UWB signals for indoor applications to -41.3 dBm/MHz which is equivalent to 75 nanowatts/MHz. Such power restriction permits UWB signals to settle underneath the noise floor of a typical narrow band receiver hence allowing them to coexist with other narrowband technologies. Following these restrictions, the FCC permits the operation of UWB devices on an unlicensed basis; hence, everyone can transmit UWB signals.

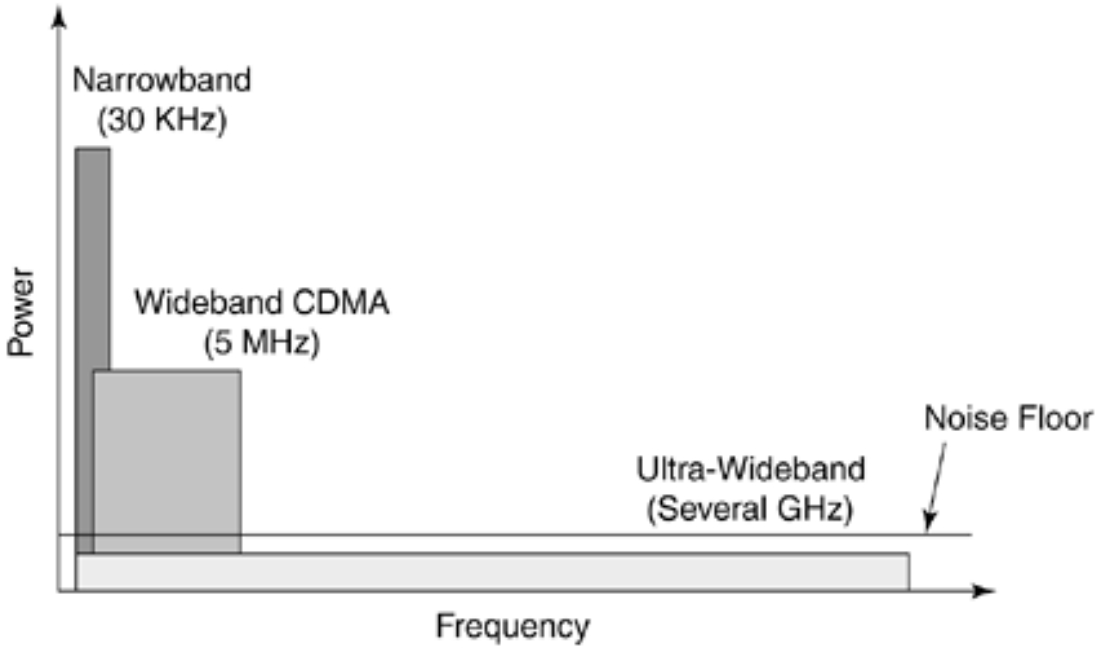

FIGURE 1.5: Coexistence of UWB signals with other narrowband services

1.1.2.2 Large Channel Capacity

Because of the huge bandwidth of UWB pulses and based on Shannon's capacity formula in (1.1), it is evident that the channel capacity is improved with UWB.

$$C = B \log_2(1 + SNR) \tag{1.1}$$

In fact, the channel capacity C has a linear dependence on the bandwidth B and it is expected to have a data rate of gigabits per second (Gbps) if combined with MIMO technology. However, due to the power limitation set by the FCC on the transmission of such signals, in order to achieve such high data rate a trade-off must be made with distance resulting with a range of up to 10 meters. Such model can provide more than 500 Mbps data transmission rate within the range of 10m [4] which renders UWB systems ideal applicants for short-range, high data rate wireless applications.

1.1.2.3 Ability to Work with Low SNR's

Based on Shannon's equation in (1.1), we can see that the relation between the channel capacity and the signal-to-nose ratio (SNR) is only logarithmic. Therefore UWB signals can perform high channel capacity even with low SNR's due to their large bandwidth.

1.1.2.4 Low Transmit Power

The limitation set by the FCC on the transmission power for UWB signals renders UWB systems very power efficient and hence will minimize the cost of implementation. And due to their large bandwidth, even at low transmit power will the system provide high data rate as explained in part 1.1.2.3. Such power efficient and low cost implementation preserve the battery life and size of the system rendering it very attractive for portable devices.

1.1.2.5 Resistance to Jamming

The information signals in UWB are spread over a large array of frequencies ranging from over several GHz's hence providing a high processing gain (PG). Process gain is the ratio of the RF bandwidth to the baseband (information) bandwidth. It is used to describe the unique properties of spread spectrum waveforms. PG is used as a measure of a radio system's resistance to jamming. Because of the frequency spread over a large range, it would be extremely difficult to jam all frequencies in the UWB spectrum at once.

1.1.2.6 High Performance in Multipath Channels

Multipath is a well-known phenomenon in wireless communication system channels. It is the result of receiving two or more paths which are caused by the multiple reflections of the transmitted signal after colliding with different objects such as trees, buildings, mountains, people, etc. The path received directly for the transmitter is known as the line of sight (LOS). The path received from the reflections is known as non-line of sight (NLOS). These reflections can cause destructive interference with the LOS received signal hence resulting in a severe degradation to the transmitted signal as shown in figure 1.6. Such effect is more serious for narrowband than for UWB signals. In UWB systems, the pulses are characterized by their short duration (in the order of nanoseconds) which results in a high temporal resolution making them very hard to collide with the LOS pulse. However, that doesn't mean that UWB communications is invulnerable to multipath rather it is more immune than the case of narrowband communications systems.

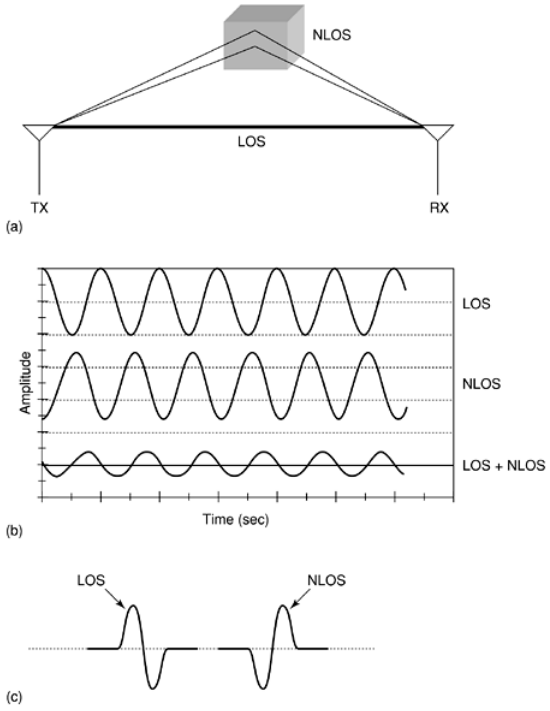

FIGURE 1.6: Effect of multipath channels

1.1.2.7 Carrierless Signal

Applying short-duration pulses as the building blocks for communications directly produces a very large bandwidth. Hence there is no need to have a carrier frequency to modulate the information signal on. This implies that UWB transceivers require fewer RF components and hence less complex than the carrier based transmission. For this reason, UWB transceiver architecture is considerably simpler and thus cheaper to build resulting in a cost-effective solution. A comparison between the transceiver architectures of narrowband and wideband systems is shown in figure 1.7

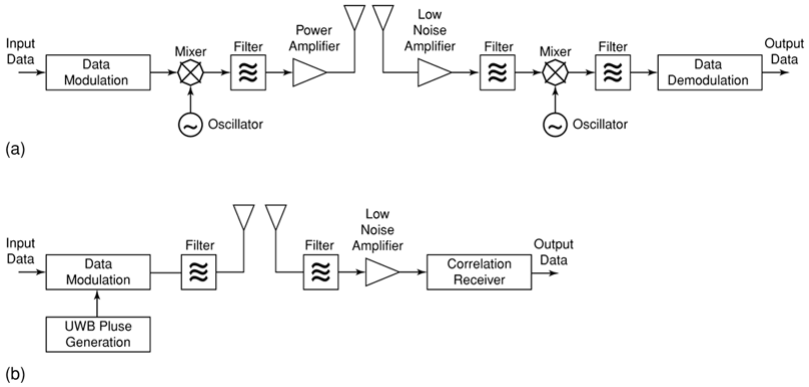

FIGURE 1.7: Transceiver architectures for narrowband and ultra-wideband systems

1.1.3 Limitations

The most limiting factor in UWB signals is the transmission power that restricts the operation range to about 10m for high data rates. Such limitation makes the synchronization and acquisition of UWB signals difficult, as tracking the very short pulses with sufficient accuracy is very challenging. While at the transmission side the architecture is simple and uses less power than narrowband transmitters, the challenge resides at the receiver side as it must be able to demodulate the incoming UWB signals in a practical way without using too much power, as simple as possible and as cost efficient as possible.

We present the main challenges of UWB communications.

1.1.3.1 Pulse-Shape Distortion

In narrowband modulation, the signals stay sinusoidal throughout the transmission channel. However, the low power UWB pulses are exposed to severe distortion by the transmission link [1]. This can be shown mathematically using Friis equation on the relation between the power received and the power transmitted by an antenna:

$$P_r = P_t G_t G_r (\frac{c}{4\pi df})^2 \tag{1.2}$$

From the above equation, it can be seen that the power of the received signal decreases quadratically with the increase in frequency. In the case of narrow frequencies such as narrowband signals, the change in frequency barely changes the received power and hence can be ignored. Nevertheless, for ultra-wideband frequencies and because of the large range of frequencies that this system covers, the received power radically fluctuates and thus distorts the shape of the pulse. Such distortion will limit the performance of UWB receivers.

1.1.3.2 Channel Estimation

In wireless communications, channel state information (CSI) refers to the characteristics of a channel in a specific transmission medium such as attenuations, scattering and delays of the propagation path. Estimating the channel's parameters makes it possible to adjust the transmitted signals to the channel conditions in order to achieve a more reliable communication with higher data rates. Estimating the parameters of a certain channel is done using training sequences sent by the transmitter and processed by the receiver. Given that most UWB receivers associate the received signal from a predefined constellation set of signals, knowing the parameters of the wireless channel in advance is essential in order to guess the received signal correctly. However, due to the pulse distortion discussed above in part (a) estimating the channel in UWB systems becomes very difficult due to the dense multipath channel (large number of multipath components).

1.1.3.3 Challenging Synchronization

The most important channel parameter required by most receivers is the carrier frequency [5]. The received carrier frequency may be different from the nominal transmitted carrier frequency value. Such deviation between the transmitted and the received carrier frequencies increases the bit error rate [5]. Time synchronization is a

main challenge in UWB communication systems. In order to optimize the error performance, time synchronization between the transmitter and the receiver is a must. However it is very challenging to sample and synchronize the pulses resulting from the UWB system which are in the order of nanoseconds. In order to sample these thin pulses, very fast analog to digital converters are required [1]. Furthermore, the firm power restrictions and narrow pulse period render the performance of UWB technology highly sensitive to timing errors such as jitter and drift [1].

1.1.3.4 Multiple-Access Interference

Ultra-Wideband technology can convey large amounts of data with low power and can deliver high data rates for short distances. Hence several transmitters can coexist in the same coverage area. Thus proper multiple access methods are required to implement the channelization for multiple users. In a communication system where multiusers coexist on the same channel, different users transmit different and independent information to a single receiver [6]. On the receiving side, the receiver must be capable to differentiate between the different users and identify information from the user of interest. Cross-correlation of unwanted user's signals on the anticipated signal due to their partial overlap is considered to be one of the major limitations that may cause severe performance degradation to both the capacity of the channel. Such interference is known as multiple-access interference (MAI) [1]. The presence of channel noise and narrowband interference can overcome the limited powered UWB pulses and make the detection process very challenging [1].

1.1.4 Types of UWB: Single Band (IR) and Multiband (OFDM)

UWB technology has presented a strong candidate for wireless personal area networks providing very high data rates over short distances. Intel, for example, believes that such technology can be used best in home or business environments due to

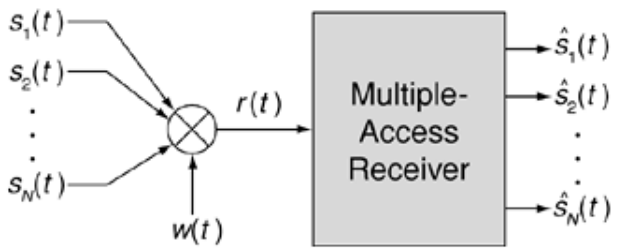

FIGURE 1.8: Multiple access receiver

its short range, allowing high data rates and equipment mobility to ease information sharing [3]. However, several techniques have been suggested in the literature regarding the technology that shall be implemented for UWB communication systems. These techniques can be classified into two major groups: single-band and multi-band [7]. The former technology backed by Motorola/XtremeSpectrum, suggests the idea of impulse response (IR) which is the conventional approach to UWB using narrow pulses in the time domain resulting in a wide frequency spectrum. The latter on the other hand, which is backed by several companies such as Intel and Texas Instrument, proposes splitting the available UWB frequency spectrum into multiple smaller and non-overlapping bands with bandwidths larger than 500 MHz [1].

1.1.4.1 Single Band (IR)

Single-band (IR) approach, also referred to as carrierless communications, is realized using narrow UWB pulses with low duty cycle to modulate the information signals which will occupy the available UWB bandwidth. Direct-sequence UWB or time-hopping spreading techniques can be used in order to support multiple users. Figure 1.9 demonstrates series of impulse signals having low duty cycle, where T_f is the frame interval, also known as the pulse repetition time, and T_w is the duration of a monocycle. Typically, T_f is 100 or 1000 times longer than the pulse width T_w [7].

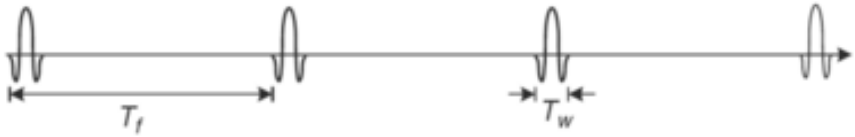

FIGURE 1.9: Sequence of impulse signals with low duty cycle

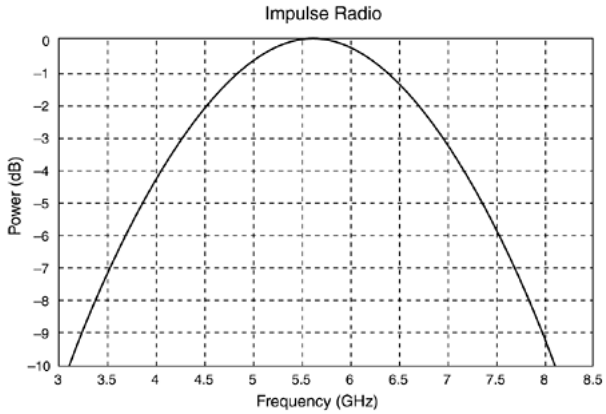

FIGURE 1.10: Narrow pulse in the frequency domain

1.1.4.2 Multiband OFDM

Multiband technique divides the 7.5 GHz available RF spectrum for UWB communications into multiple sub-bands each having a bandwidth greater than 500 MHz. Figure 1.11 depicts the result. Dividing the UWB spectrum into several frequency bands avoids the interference over certain pre-allocated bands. In such modulation, the UWB pulses are not as narrow as in the case of IR single band approach; hence, synchronization requirements are more relaxed [1].

Both techniques, single band and multiband, are valid and remarkable. As the latter solves the interference problem with other bands, it requires more complexity; whereas, the former offers better coexistence with other radio services but introduces possible interference.

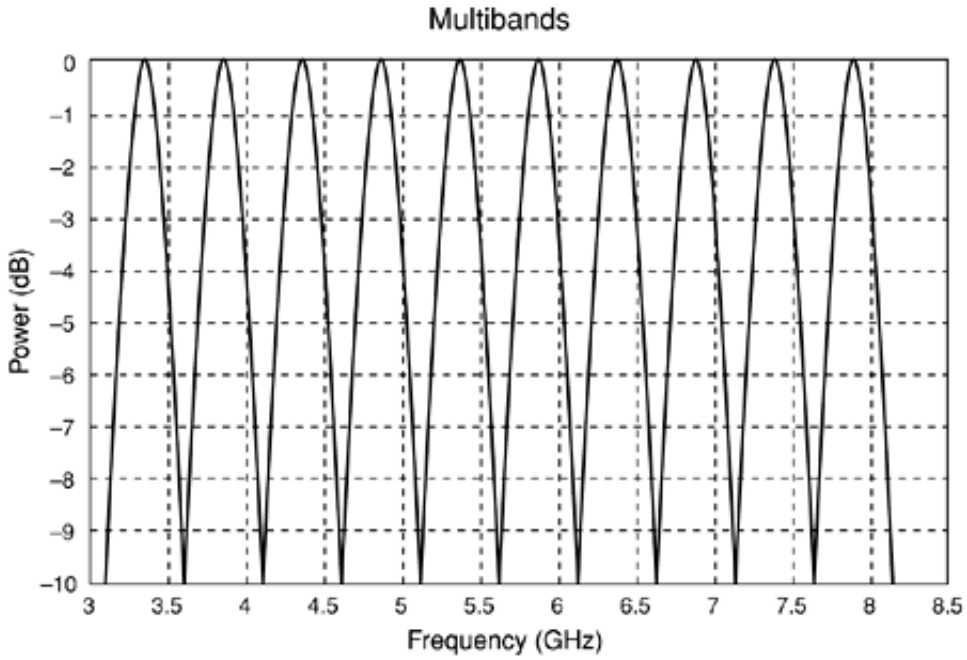

FIGURE 1.11: Multiband frequency spectrum

1.1.5 PPM Modulation

Several modulation techniques have been investigated and thoroughly analyzed in the literature of indoor UWB systems such as pulse amplitude modulation (PAM), on-off keying (OOK), phase shift keying (PSK) and pulse position modulation (PPM) [7]. However, because UWB systems modulate very low duty-cycle pulses (in the order of sub-nanoseconds) where it is very hard to control their amplitude and phase, unipolar transmissions are desirable for such systems. PPM takes advantage of UWB high temporal resolution and high peak-to-average power ratios in order to modulate such systems [8].

1.1.5.1 Concept

Pulse position modulation (PPM) is an orthogonal baseband modulation technique which lies under isochronous modulation along with PWM (pulse width modulation) and they both belong to the pulse time modulation family, refer to figure 1.12. Such

modulation techniques are set to be isochronous because of the equal sampling rate such schemes provide disregarding the frequency and amplitude of the modulation signal. Hence, the sampling rate is exclusively determined by the selected carrier [9]. In PPM, the position of the pulse is altered according to the sampled value of the information signal; hence, the information is carried by varying the position of the pulse within a constant time window. M-PPM on the other hand modulates digital information signal (PCM data) into a single pulse occupying a specific time slot out of the M slots. In M-PPM, a key time partition (window) is divided into M time slots (or chips) each with a constant time duration T_c. A symbol consists of a single narrow pulse taking position in one of these slots. K-bits of information are mapped into one of the $M = \log_2 K$ distinct slots symbols while the other M-1 chips remain empty [10]. The idea of PPM is to change the position of the pulse to denote different symbols. Figure 1.13 illustrates the different PTM techniques

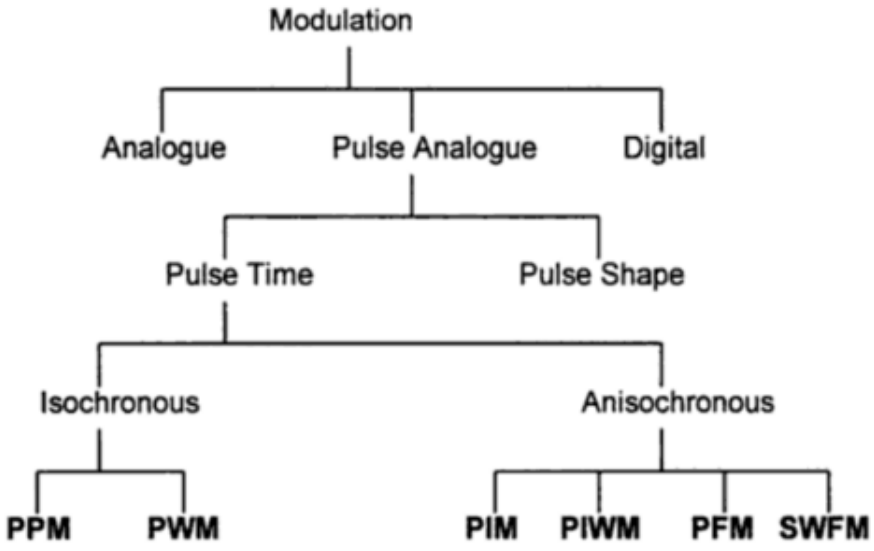

FIGURE 1.12: PTM classification system

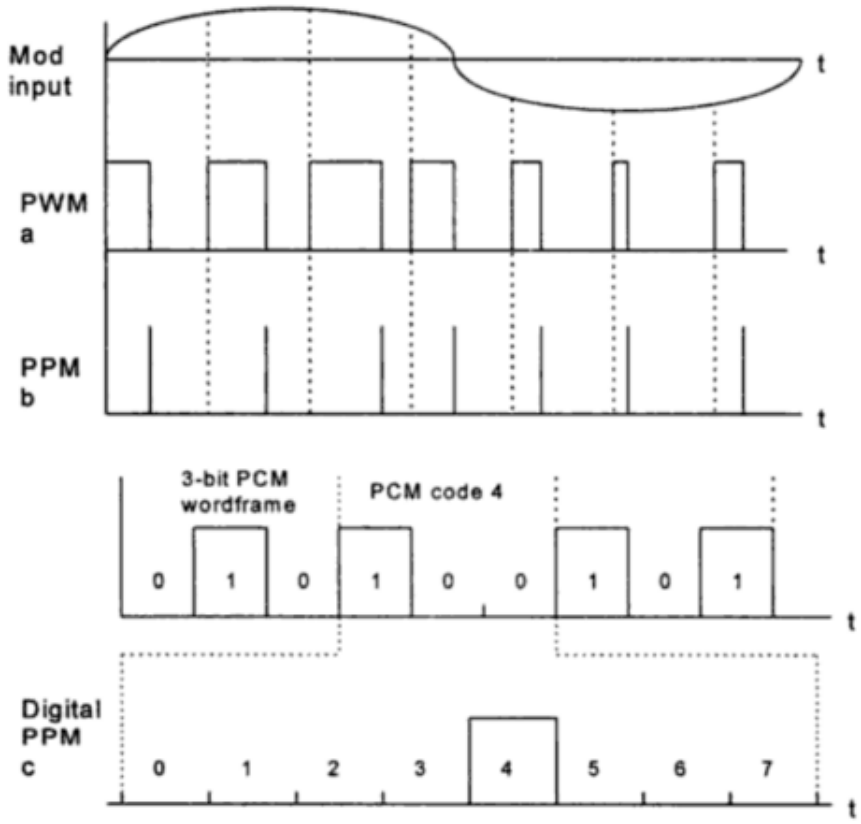

FIGURE 1.13: Isochronous PTM techniques

1.1.5.2 Advantages

The main advantage of M-PPM lies in its high power efficiency compared to other baseband modulation schemes which makes it a great candidate for UWB systems giving the power restriction accompanied with such technology.

1. Power Efficiency

   M-PPM pulses have low duty cycle, equal to $\frac{1}{M}$; hence they offer high pulse intensity and low average power making it well suited for low transmission power transmitters [11]. Moreover, PPM pulses require constant transmitting power since they are of constant amplitude and duration. In UWB systems, pulses are of a narrow nature, typically their duty cycle is less than 0.5% [1].

2. High Temporal Resolution

   Given the ultra-wide bandwidth of UWB pulses, Pulse Position Modulation (PPM) takes advantage of the high temporal resolution associated with such systems. Being a carrierless transmission technology, it is hard to control the amplitude and phase of the IR-UWB pulses thus making it ideal for unipolar PPM.

3. Enhanced Performance level

   In M-ary PPM, the M-slots (ships) are non-overlapping in time; hence, each symbol is orthogonal to all others. In other words, the dimension of the constellation signal space is M and are represented as an M dimensional Euclidean space with a single constellation point on each of the M axes. This results in an increase of the performance level with the order of M.

1.1.5.3 Limitations

In M-PPM, three main steps are required in the demodulation process. The first step involves finding the slot boundaries and frequency. The second step consists of identifying the slot frequency, The final and most vital step is knowing in which slot the pulse resides [12]. Thus synchronizing a PPM signal in order to properly reconstruct information is very challenging [12].

1.1.6 Applications

The trade-off between range and data rate in UWB systems opens a wide door for different applications in many sectors such as military, civilian and commercial sectors [1]. The FCC classifies UWB applications as either imaging, radar or communications devices [3].

1.1.6.1 Localization Systems

Localization systems such as Global Positioning Satellite (GPS) require the use of time to process signals to allow fine positioning. The direct relationship between bandwidth and precision makes UWB systems extremely efficient in locating objects (millimeter and even sub-millimeter resolution) [13]. More bandwidth will increase positioning measurement precision [13].

1.1.6.2 Radar Systems

Radar is considered one of the most significant applications of UWB. The ultra-narrow pulses provided by such technology allow fine positioning with a great resolution (within centimeters) to identify the position and movement of objects [1] [13]. Moreover, and because of the ultra-wide range of frequencies offered by such system, UWB signals can easily penetrate different obstacles which can be used in various applications such as:

- Rescue operations for detecting survivors stuck under wreckage
- Locate pipes, studs and electrical cabling
- Remote heart monitoring in medical imaging
- Automotive industries such as collision avoidance, smart airbags, precision surveying, automotive sensors, etc. [13]

1.1.6.3 Data Communications Systems

The ability of UWB systems to provide high data rates along short distances nominate them to be a great candidate for home and business networking applications in the

form of Wireless Personal Area Network (WPAN). Freeing people from cables, allowing the transfer of information such as video, audio and high bandwidth data at data rates reaching gigabits per second [13] is the great advantage of such technology.

1.1.7 UWB Channel Model

In order to design wireless transmitters and receivers, the main building blocks of any wireless communication system, knowledge of the channel is required to establish an appropriate design. The occurrence of multipath components in an indoor environment makes it difficult to model such channel. In addition the received narrow pulses at the receiver arriving from the UWB signals from different paths need to take into account the time varying properties resulting from such paths.

1.1.7.1 Cluster-Ray Model and Basic Parameters

Various measurements have been proposed in the literature concerning indoor wireless communication channels [14]. The channel model followed in this work is the modified Saleh Valenzuela channel model proposed by [15] and [16].

The original model described by Saleh and Valenzuela (SV model) explains that the received pulses arrive in separate clusters of rays [14]. The rays are a result of the delayed echoes of the initial pulse. Their results are based on an empirical experiment carried out in indoor environments in 1987 [14]. Figures 2.7 clearly demonstrate the cluster model.

The SV model describes the arrival times of the clusters' rays as two independent Poisson processes with rates Λ and λ respectively. Whereas the path voltage gains correspond to the Rayleigh probability density function as shown in equations (1.4).

$$p(T_l|T_{l-1}) = \Lambda \exp[-\Lambda(T_l - T_{l-1})], \text{ where l>0} \tag{1.3a}$$

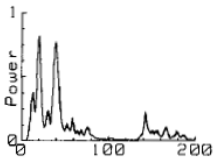

(A) impulse response of a narrowband signal showing two separate clusters

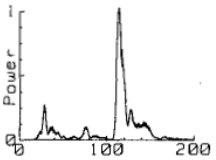

(B) impulse response of a narrowband signal showing one cluster 100ns delayed significantly stronger than the previous one

FIGURE 1.14: two examples of frequency-average power profiles

$$p(\tau_{kl}|\tau_{(k-1)l}) = \lambda \exp[-\lambda(\tau_{kl} - \tau_{(k-1)l})], \text{ where k>0} \tag{1.3b}$$

$$p(\beta_{kl}) = (2\beta_{kl}/\overline{\beta_{kl}^2}) \exp(-\beta_{kl}^2/\overline{\beta_{kl}^2}) \tag{1.3c}$$

The modified channel model, which is based on the SV model, uses a similar channel model but yet better fits the observed data. Instead of the independent Rayleigh model of the amplitude gains of the fading paths a log-normal distribution is proposed [15][17].

$$h(t) = x \sum_{n=1}^{N} \sum_{k=1}^{k(n)} \alpha_{nk} \delta(t - T_n - \tau_{nk}) \tag{1.4}$$

Where:

x = log normal random variable indicating the amplitude gains of the fading paths

N = number of clusters

$K(n)$ = number of multi-path contributions within the n_{th} cluster

α_{nk} = coefficient of the k_{th} multipath contribution of the nth cluster

T_n = arrival time of the n_{th} cluster

τ_{nk} = delay of the k_{th} multipath contribution within the n_{th} cluster

This channel model has been adopted in the IEEE 802.13a channel model recommendation.

1.1.7.2 Model Parameters

Based on the channel's conditions, the modified SV model provided 5 different situations:

1. CM1: LOS (Line of Sight) from 0-4m distance

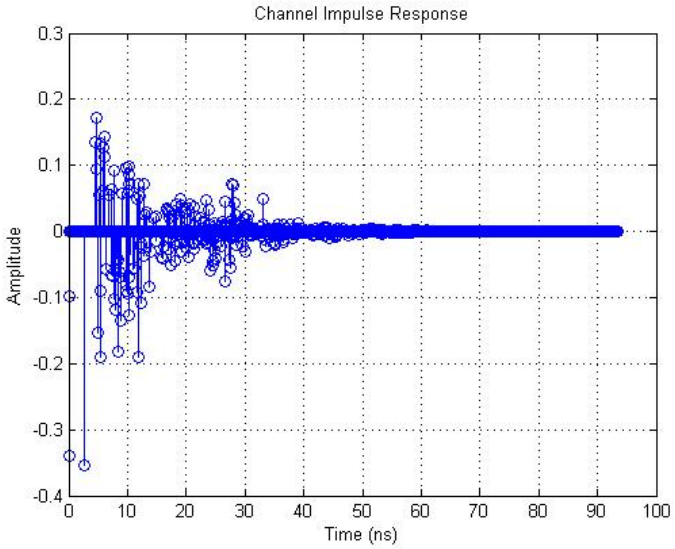

FIGURE 1.15: Channel impulse response (CM=1)

2. CM2: NLOS (Non Line Of Sight) from 0.4m distance

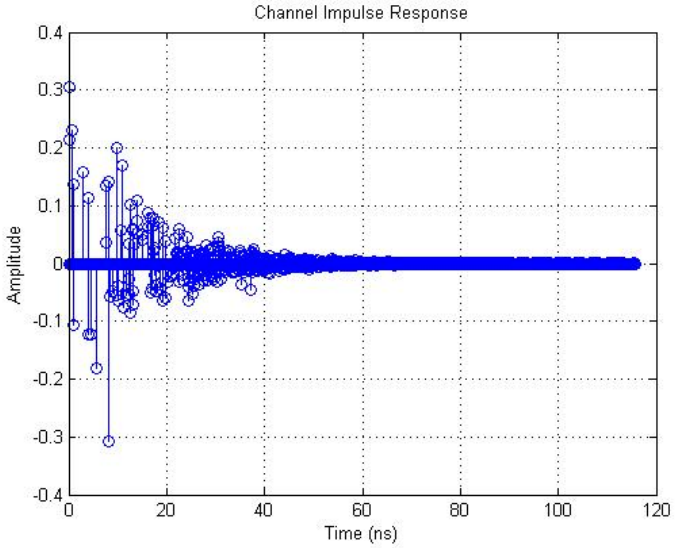

FIGURE 1.16: Channel impulse response (CM=2)

3. CM3: NLOS from 4-10m distance

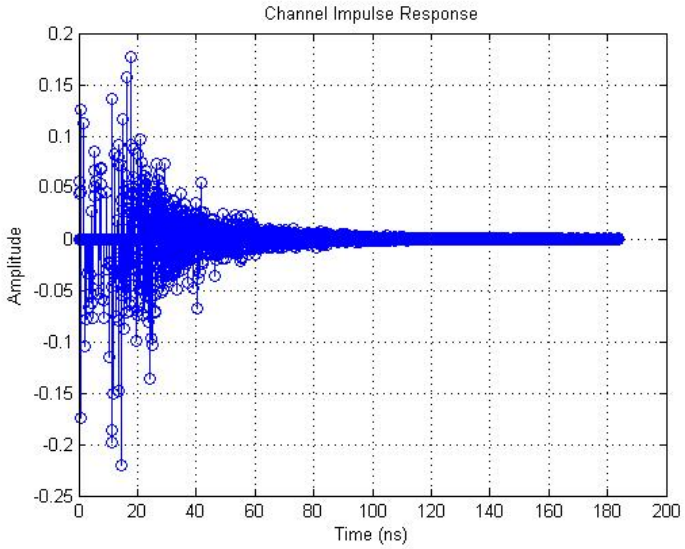

FIGURE 1.17: Channel impulse response (CM=3

4. CM4: NLOS with 25ns RMS spread bad multipath channel

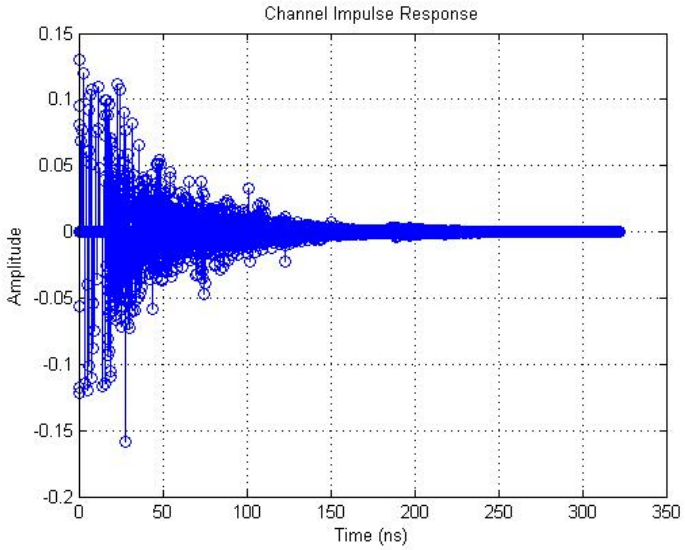

FIGURE 1.18: Channel impulse response (CM=4)

5. CM5: NLOS with 25ns RMS spread extremely bad multipath channel

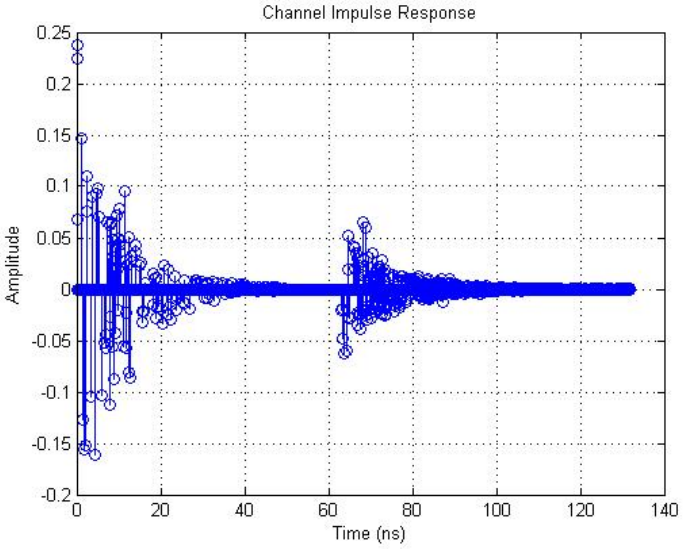

FIGURE 1.19: Channel impulse response (CM=5)

From the above different channel types, we observe the following:

- **Large number of multipath components:** Because of the reflections (scattering) of the UWB pulses in indoor environments, the channel is characterized by rich multipath components that are illustrated by the received rays in the above figures. This is shown more clearly in the case where there is no line of sight particularly for CM=5 where two different clusters appear due to reflections with different objects.
- **Delay spread:** It can be seen that the impulse response of UWB systems span a time delay of approximately 100ns.
- **Resolvable rays:** Even with a rich multipath environment, UWB pulses tend not to overlap with each others in time because of the ultra short pulse duration making it possible to resolve these pulses with different techniques such as time gating.

1.2 MIMO Systems and Space-Time Coding

1.2.1 MIMO Systems

Shannon's famous formula shows that in order to increase the channel capacity one must radiate more power or use a wider electromagnetic band. However, increasing the transmission power or using a larger bandwidth is extremely expensive since they require governmental licenses.

Lately, studies have shown that such capacity can be increased without necessarily neither increasing the transmission power nor occupying a wider bandwidth. Such techniques consist of using multiple antennas at either or both the receiver and transmitter sides taking advantage of the scattering channel and the multipath environment. This technology is known as smart antenna technology or MIMO systems. MIMO systems were introduced by Foschini and Telatar in the mid 1990's where it was proven that, for a given power and bandwidth, the capacity of the channel can be increased by increasing the number of antennas.

1.2.1.1 Concept and System Model

The architecture of MIMO systems consist of deploying multiple antennas at the transceivers. In such configuration, multiple antennas are employed at the transmitter side where the antennas transmit either the same signal or different independent signals. And at the receiver side, different antennas collect the incoming energy received and then combine them tracking the variation of the channel hence increasing the capacity [16]. Figure 1.20 illustrates the different antenna architectures: Single-Input Single-Output (SISO), Single-Input Multiple-Output (SIMO), Multiple-Input Single-Input (MISO) and Multiple-Input Multiple-Output (MIMO).

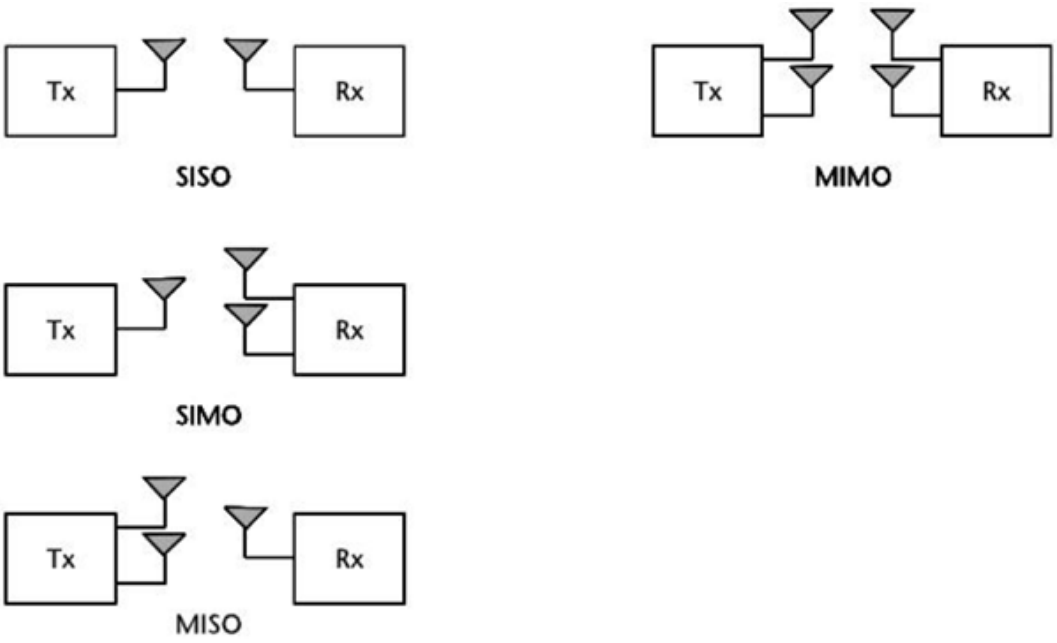

FIGURE 1.20: Different antenna architectures

1.2.1.2 Motivation

As previously mentioned, the main idea behind having a MIMO system is increasing the channel capacity without widening the bandwidth or increasing the transmission power. Hence the objective of such system is to increase the data rates through multiplexing and/or to improve performance through diversity. Whether data rates or diversity gains are to be achieved, a trade-off exists between the two.

1. **High Data Rate**

   It can be shown that the capacity of a wireless channel having a Rayleigh fading characteristics with perfect Channel State Information (CSI) at the receiver is proportional to the minimum number between the transmit and the receive antennas, min (M, N) where M is the number of transmit antennas and N is the number of received antennas [16], [18].

$$C = min(M, N) \tag{1.5}$$

This linear increase of the capacity linked with MIMO channels is built on the multipath environment provided by the channel. Such scattering environment provides independent transmission paths from each transmitter to each receiver [16]. The below illustrates a comparison between a SIMO system and a MIMO system. It clearly shows the linear increase in capacity in the case of MIMO system; whereas, a logarithmic increase for the case of SIMO.

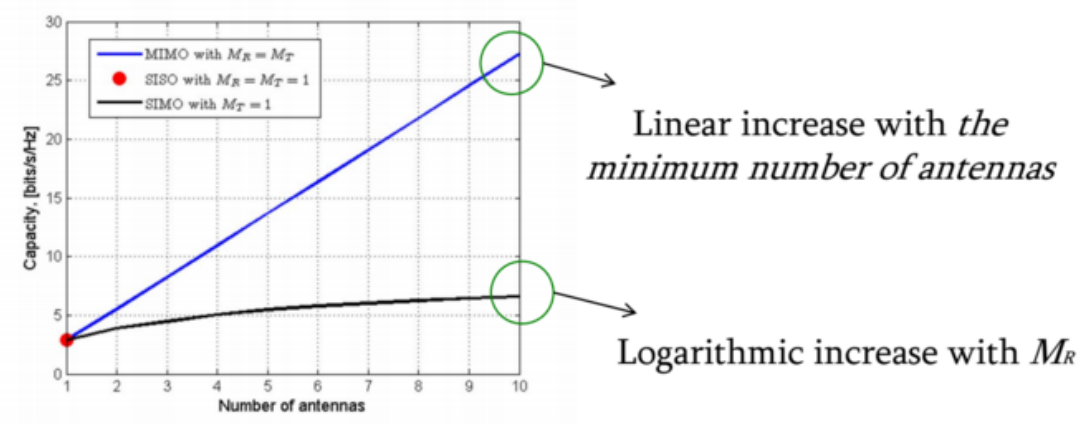

FIGURE 1.21: capacity growth of SIMO vs MIMO

2. **Antenna Diversity**

Multipath fading is one of the major problems in communication systems. Severe fading may arise to the propagated signals in a fading channel; hence, fluctuating their strength. When a signal's power falls considerably, the channel is known to be in deep fade. One of the best methods to combat such fading channels is spatial diversity [19]. Antenna diversity can be categorized under the following spatial diversity:

a **Receive Diversity:** Several antennas are employed at the receiver side in order to collect the incoming signals; hence enhancing the quality of the received signal.

b **Transmit diversity:** Several antennas are employed at the transmitter side that transmits uncorrelated replicas of the signal on independent fading branches.

Such techniques offer a powerful tool for achieving reliable communication over fading channels. It is worth mention that there exist other diversity techniques such as time and frequency diversity where the transmitted replicas of the signals are provided across the time and frequency dimensions, respectively. In the context of our work, our model is built on a transmit diversity scheme with 2 transmitters. For $M_T \times M_R$ MIMO systems with $M_T \geq 2$; spatial diversity is extracted through what is referred to as space-time coding.

1.2.2 Space-Time Coding

The term Space-Time Code (STC) was originally suggested in 1998 by Tarokh et al. to describe a new two-dimensional way (time and spatial) of encoding and decoding signals transmitted over wireless fading channels using multiple transmit antennas [20]; hence, providing replicas of the transmitted signals over both time and space. In October 1998, Alamouti was the first to design an orthogonal space-time block code (STBC) scheme with two transmitters and one receiver that achieves a full transmit diversity. Orthogonal STBCs are a generalized version of Alamouti scheme which can achieve full transmit diversity specified by the number of transmit antennas [21]. And later STBC became the core idea of MIMO systems.

1.2.2.1 Concept

Space-Time coding is a transmit diversity technique in MIMO technology. With space-time coding it is possible to transmit several independent signals simultaneously from different transmitters without prior knowledge to the channel's parameters [22]. The signals are represented as a matrix where its columns refer to the transmitter antenna and its rows refer to the time slot the signal is being sent at (figure 1.22). Once the signals are sent, a combiner at the receiver side combines the received signals where they will be processed at the maximum likelihood detector (ML) for decoding.

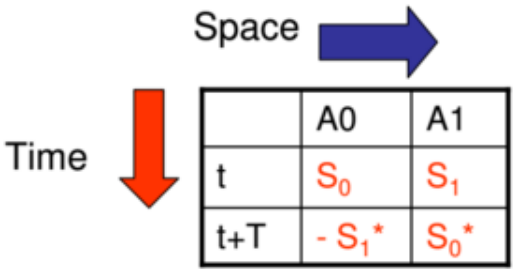

FIGURE 1.22: Space-Time Block Code matrix

STC hence introduces temporal and spatial correlation into the signals transmitted from different antennas without increasing the total transmitted power and hence increasing the reliability of the system.

1.2.2.2 Motivation

In order to measure the performance of a STBC, two important criteria have to be looked at: diversity gain and coding gain. These two measurements decide the reliability of the system.

1. **Diversity Gain (Rank criterion)**

   As described earlier in section 1.2.1, diversity in wireless communication systems is one of the best techniques to combat channel fading where multiple appearances of the transmitted signal are provided over independent channel's paths. As the number of these branches increases, the probability of receiving at any time a signal going through a fade path will decrease; hence stabilizing the wireless link and improving its quality. The maximum diversity obtained in a MIMO system is $M_t M_r$ where M_t and M_r stand for the number of transmit and receive antennas respectively. However and in order to achieve such diversity, the STBC should have a full rank as expressed in eq. (1.6) [22] [23]. Such characteristic can be translated as the asymptotic slope of the SER versus SNR logarithmic graph. Figure 1.23 demonstrates that as the diversity gain (diversity

order) increases, the slope becomes steeper.

$$\max \min_{S_i, S_j \in C;\ i \neq j} \{Rank(S_i - S_j)\} \tag{1.6}$$

2. **Coding Gain (Determinant criterion)**

   Coding gain results from how symbols are correlated across transmit antennas. In order to achieve high coding gain the determinant of the input matrix pairs (S_i and S_j) should be minimized as shown in eq. (2.7) [24]. The coding gain affects the horizontal shift of the graph as shown in figure 1.23. The higher the coding gain, the more the graph shits to the left.

$$\max \min_{S_i, S_j \in C;\ i \neq j} \left\{ \det(S_i, S_j) = \det\left[(S_i - S_j)(S_i - S_j)^H \right] \right\} \tag{1.7}$$

   Where H stands for the transpose complex conjugate.

Following from the above, the rank criterion has more impact on the performance and hence, the diversity gain is optimized first. After maximizing the diversity gain, the optimization needs to target the coding gain.

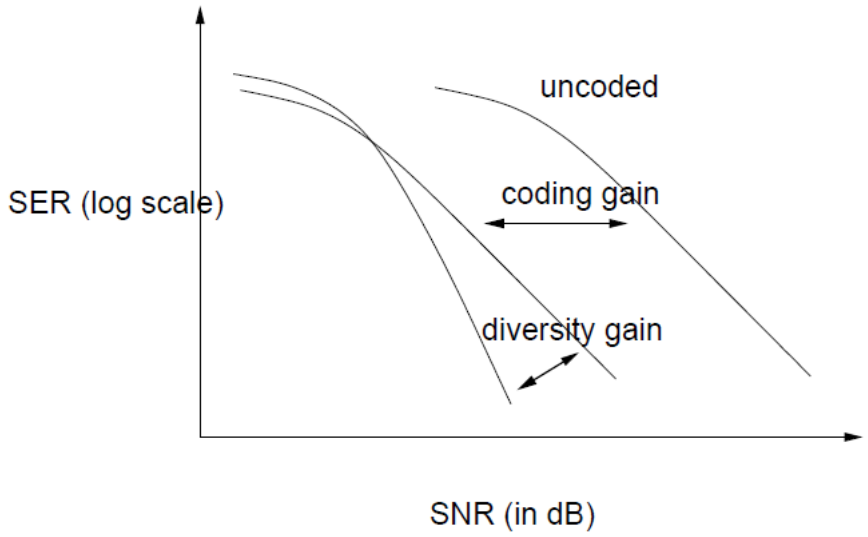

FIGURE 1.23: Diversity and Coding gains

1.2.2.3 Alamouti Code

Alamouti was the first to introduce a space-time block code for a system with two transmit antennas and one receive antenna. Using such model, his structure offers the same diversity order as maximal-ratio receiver combing (MRRC) with one transmit antenna and two receive antennas [25].

In his work, the encoded information signals are transmitted based on the following 2x2 STBC matrix:

$$s = \begin{bmatrix} s_1 & s_2 \\ -s_2^* & s_1^* \end{bmatrix} \tag{1.8}$$

Where s_1 and s_2 are two independent information messages carved from the selected constellation. They are the signals transmitted from the first and the second antenna respectively as shown in figure 1.24. The fading coefficients of the channels are as-

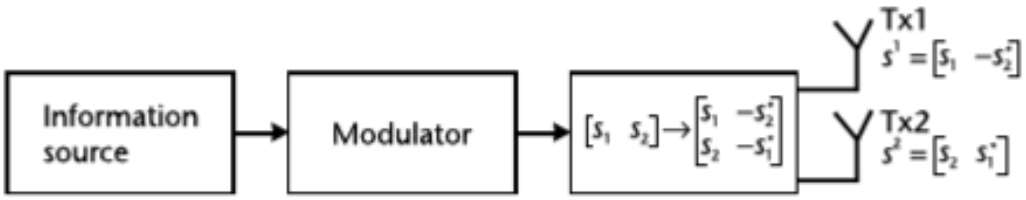

FIGURE 1.24: Alamouti space time encoder

sumed constant over two successive symbol transmission periods and are characterized as follows:

$$h_1(t) = h_1(t+T) = h_1 = \alpha_1 e^{j\theta_1} \tag{1.9a}$$

$$h_2(t) = h_2(t+T) = h_2 = \alpha_2 e^{j\theta_2} \tag{1.9b}$$

Given two symbols s_1 and s_2. Based on Alamouti space-time code, the transmitted symbol over the first time interval (t) by the first and second transmitter respectively

is $\binom{s_1}{s_2}$. The received symbol y_1 is given as:

$$y_1 = \begin{bmatrix} h_1 & h_2 \end{bmatrix} \begin{bmatrix} s_1 \\ s_2 \end{bmatrix} + w_1, \text{ where } w_1 \text{ stands for the Gaussian noise} \tag{1.10}$$

In the second transmit period (t+T), the first antenna the symbol transmitted is $-s_2^*$ and from the second transmitter s_1^* is transmitted. Hence the received symbol in the second transmit period become:

$$y_2 = \begin{bmatrix} h_1 & h_2 \end{bmatrix} \begin{bmatrix} -s_2^* \\ s_1^* \end{bmatrix} + w_2, \text{ where } w_2 \text{ is a Gaussian noise vector} \tag{1.11}$$

Expanding (1.10) and taking its conjugate will result in the following:

$$y_2 = -h_1 s_2^* + h_2 s_1^* + w_2 \tag{1.12a}$$

$$\begin{aligned} y_2^* &= -h_1^* s_2 + h_2^* s_1 + w_2^* \\ &= \begin{bmatrix} h_2^* & -h_1^* \end{bmatrix} \begin{bmatrix} s_1 \\ s_2 \end{bmatrix} \end{aligned} \tag{1.12b}$$

Following from eq. (1.9) and eq. (1.11b):

$$\begin{bmatrix} y_1 \\ y_2^* \end{bmatrix} = \begin{bmatrix} h_1 & h_2 \\ h_2^* & -h_1^* \end{bmatrix} \begin{bmatrix} s_1 \\ s_2 \end{bmatrix} + \begin{bmatrix} w_1 \\ w_2^* \end{bmatrix} \tag{1.13}$$

Denoting the matrix having the channel's parameters in (1.12) by H, the following can be observed:

$$\begin{aligned} H \times H^H &= \begin{bmatrix} h_1 & h_2 \\ h_2^* & -h_1^* \end{bmatrix} \begin{bmatrix} h_1^* & h_2 \\ h_2^* & -h_1 \end{bmatrix} \\ &= \begin{bmatrix} h_1 h_1^* + h_2 h_2^* & h_1 h_2 - h_1 h_2 \\ h_1^* h_2^* - h_1^* h_2^* & h_1 h_1^* + h_2 h_2^* \end{bmatrix} \\ &= \begin{bmatrix} |h_1|^2 + |h_2|^2 & 0 \\ 0 & |h_1|^2 + |h_2|^2 \end{bmatrix} \end{aligned} \tag{1.14}$$

Where H^H stands for the Hermitian (transpose conjugate) of the matrix H.

Based on the result in eq. (1.13), it can be easily observed that the matrix H is orthogonal. Such property makes the decoding part simple as it requires a linear operation to remove the interference caused by one symbol over the other following eq. (1.14) (figure 1.25);hence, the following:

$$\begin{aligned} \begin{bmatrix} z_1 \\ z_2 \end{bmatrix} = H^H \begin{bmatrix} y_1 \\ y_2^* \end{bmatrix} &= H^H H \begin{bmatrix} s_1 \\ s_2 \end{bmatrix} + H^H \begin{bmatrix} w_1 \\ w_2^* \end{bmatrix} \\ &= (|h_1|^2 + |h_2|^2) I_2 \begin{bmatrix} s_1 \\ s_2 \end{bmatrix} + \begin{bmatrix} w_1' \\ w_2' \end{bmatrix} \end{aligned} \tag{1.15}$$

Where I_2 is the 2×2 identity matrix and $\begin{bmatrix} w_1' \\ w_2' \end{bmatrix}$ is the new noise term. The ML decoder decides in favor of $(\tilde{s_1}, \tilde{s_2})$ which are decoded separately based on the following rules:

$$\tilde{s_1} = \arg \min_{s_1} \left(z_1 - (|h_1|^2 + |h_2|^2) s_1 \right)^2 \tag{1.16a}$$

$$\tilde{s_2} = \arg \min_{s_2} \left(z_2 - (|h_1|^2 + |h_2|^2)s_2\right)^2 \tag{1.16b}$$

Hence Alamouti code is known as an **Orthogonal Space-Time Block Code** (OSTBC).

Alamouti code provides the following attractive characteristics:

1. For any signal constellation, it achieves the maximum transmit diversity order of $d_{max} = 2$.
2. The transmitter does not need to know the characteristic parameters of the channel.
3. Being an orthogonal code, linear decoding can be applied in order to decode the received signals.

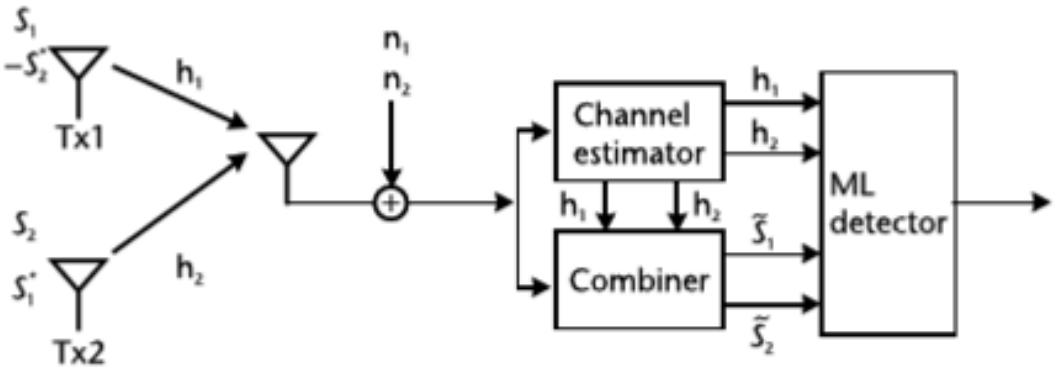

FIGURE 1.25: Alamouti space time decoder

1.3 Coherent, Non-Coherent and Differential Systems

In the past years, intensive works on designing codes for achieving transmit diversity over the wireless channel were discussed. Following this premise, all of the work was focused on the case where the receiver has a perfect knowledge of the channel's parameters which is the case of most practical systems. The first proposed scheme

was by Wittneben which covers a delay diversity scheme [26]; later Foschini introduced the architecture of space-time code [27] and in 2000 Tarokh and Jafarkhani introduced differential encoding that doesn't require knowledge of the channel at neither the transmitter nor the receiver. Other techniques such as energy detectors and transmitted-reference signaling are also found in the literature which also does not require any knowledge of the CSI [28] [29] [30] [31] [32].

In IR-UWB systems, the energy of the ultra-short transmitted pulses is spread over a huge number of multipath components. Thus in order to collect a sufficient amount of energy, the receiver should be able to intercept as much as multipath components. This task can be carried out either coherently, noncoherently or differentially.

Due to the nature of UWB, narrow pulses and low transmission power, designing a receiver circuit for such system is complicated and requires high power consumption [33]. Converting UWB signals from analog to digital involves a high sampling rate and consumes a lot of power given the large bandwidth of the transmitted signals.

1.3.1 Coherent Systems

1.3.1.1 Concept

In coherent systems, the channel state information (CSI) is known at the receiver side. In general, the CSI estimation is accomplished by using pilot symbols that are transmitted along with the data and are known to the receiver [34]. In order to have an accurate estimation, a large number of channel's parameters must be estimated; hence rendering the system more complex. In general Rake receivers are used with a large number of fingers to collect significant amount of energy by estimating the gains and delays of the paths received. Afterwards the arriving waveform is correlated with a local replica (template) of the channel response. Figure 1.26 represents the block diagram of a rake receiver where the outputs are first sent through a delay line before

entering the diversity combiner due to the time shifting property introduced by the channel as a result of its multipath environment.

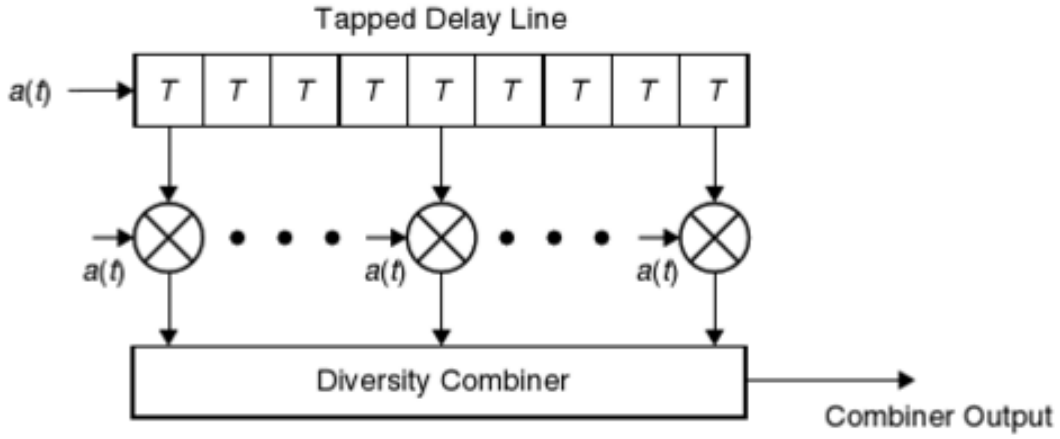

FIGURE 1.26: Rake receiver

1.3.1.2 Estimation of The Received Signal

Based on the fact that the receiver has a perfect knowledge of the CSI and using Rake receivers to collect the transmitted pulses, several techniques can be adopted to combine the received signals such as selection combiner, maximal ratio combiner (MRC) and equal gain combiner (EGC).The goal of the combiner is to improve the noise performance of the system.

1. **Selection Combiner**

   In the selection combiner, the combiner selects the channel or path that has the highest SNR value. It is assumed that the received signals from each branch are independent. In the case of indoor channels, the transmitted signal is subject to reflections which results in several independent echoes received at the receiver.

2. **Maximal Ratio Combiner (MRC)**

   In selection combiner, $(N-1)$ elements of the array of signals are ignored which makes such technique not the optimal solution. In maximal ratio combining

however, N signals from each path are multiplied by a weight factor that is proportional to their signal to noise ratio and then summed. Hence, branches with strong signal are further amplified, while weak signals are attenuated. It can be shown that the SNR at the combiner output equals the sum of the SNR of the branches [35].

$$SNR_{MRC} = \sum_{n=1}^{N} SNR_n \tag{1.17}$$

3. **Equal Gain Combiner (EGC)**

   It is similar to MRC with the weights of the paths are set to have a unity magnitude. Despite being considerably simpler to implement, the EGC results in an enhancement in SNR that is comparable to the optimal maximal ratio combiner.

1.3.1.3 Advantages

Implementing a coherent receiver with an accurate channel estimator allows to reconstruct the transmitted signal more accurately, increasing the performance of the system and enhancing the SNR. Evidently, the system complexity is compromised.

1.3.1.4 Limitations

The main limitations for coherent receivers are the increased complexity and the power consumption of such systems. The complexity arises from the need to acquire a good estimate of the channel in order to generate accurate results. Such digital topologies are not power efficient in UWB systems due to the excessive sampling rates required and the amount of data that have to be processed by the DSP [36]. In addition, coherent UWB systems require the use of coherent rake receivers with a large number of rake fingers due to the large delay spread introduced by the UWB channel thus

consuming more power and increasing the complexity [33]. Another challenging limitation of such systems is the pilot symbols that are used in order to estimate the channel's parameters. In order to have a better estimation of the channel, the number of pilot bits should be increased, giving rise to a clear trade-off between estimation accuracy and bandwidth efficiency [34].

1.3.2 Non-Coherent Systems

1.3.2.1 Concept

In non-coherent receivers, no channel estimation (CSI) or correlators are required. One way to reconstruct the transmitted signal is based on energy detection. This approach requires the use of integrators to collect the energy and detect the incoming pulses.

1.3.2.2 Estimation of The Received Signal

1. **Energy Detection**

   In M-PPM UWB systems where the symbol is transmitted in one of the M slots, the receiver perceives the energy in each of the M slots. This is done by first squaring the received pulses as shown if figure 1.26 and then passed by a windowed integrator to calculate the energy. The squarer is computed over a time window T_1, T_2; hence modifying this window allows more or less energy to be assigned in a specific window. Setting T_1 and T_2 is done through a comparator. In our work, the window is set to be 10 ns; thus we are computing the energy of the first 10 ns of each M-PPM slot. Afterwards, a maximum likelihood detector decides in which position the symbols were transmitted based on the maximum energy detected in the slots.

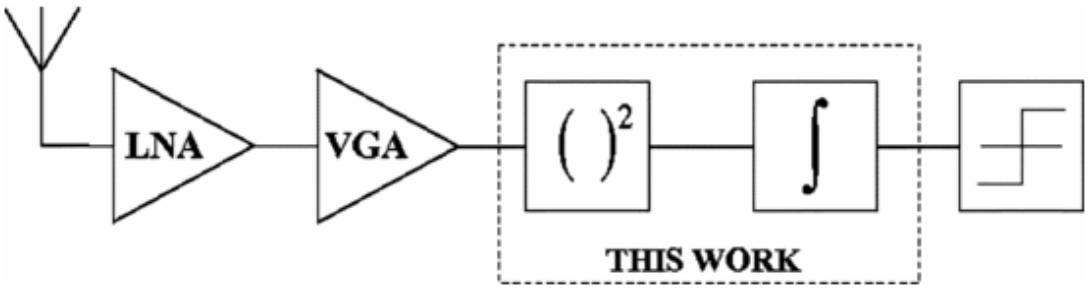

FIGURE 1.27: Energy detection architecture

1.3.2.3 Advantages

Non coherent detection is a promising technique for low complexity and low power consumption systems. The main advantage over coherent detection is that the hardware complexity is well reduced. This leads to great performance in terms of power consumption. Avoiding the implementation of Nyquist rate ADCs and power-hungry DSPs running at full speed to process the received signal reduce both the hardware complexity and the power consumption. Evidently, no training nor channel estimation procedures need to be implemented.

1.3.2.4 Limitations

Because the channel is unknown at the receiver, the signal to noise ratio (SNR) of such receivers is inferior to that of the coherent ones. The BER performance of such systems depends on the integration window time, which determines the amount of signal energy gathered during the integration period [33]. In addition such systems undergo spectral efficiency reduction, higher sensitivity to co-channel interference, and lower capability to exploit the multipath channel diversity compared to coherent detectors [37].

1.3.3 Differential Systems

1.3.3.1 Concept

Differential systems lie under non-coherent detection where the channel is unknown at both the receiver and the transmitter. For MIMO systems, differential space-time codes are an extension of the differential phase-shit keying (DPSK) introduced in SISO systems.

1. **Differential Phase Shift Keying**

   Differential phase shift keying (DPSK) is widely used in single antenna architectures (SISO) when the CSI is unknown to both the receiver and the transmitter and it assumes that the channel remains constant between two consecutive symbol durations.

   Figure 1.29 illustrates the modulation process for a DPSK scheme. First an arbitrary reference bit is chosen (example '1'). The encoding then starts according to the following rule:

   $$d_k = a_k \oplus d_{k-1} \tag{1.18}$$

   The encoding rule can be summarized as follows:

   - If d_k and d_{k-1} are the same, then they represent a 1 of a_k
   - If d_k and d_{k-1} are different, then they represent a 0 of a_k

   The sequence of d_k is then modulated onto a carrier with phase 0 or π.

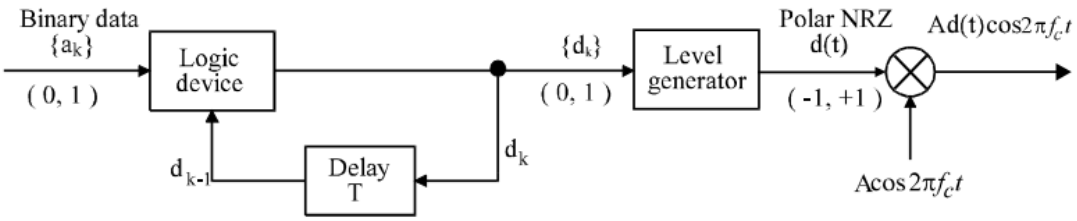

FIGURE 1.28: DPSK modulation diagram

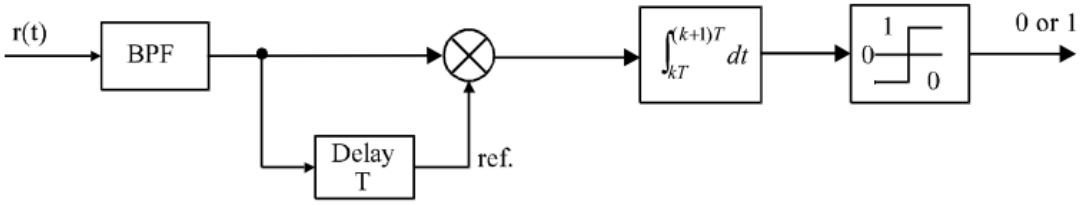

FIGURE 1.29: DPSK demodulation diagram

The demodulation multiplies both successive symbols and decides in favor of the sign of the multiplication. In fact, This is because the output of the integrator is given by:

$$l = \int_{kT}^{(k+1)T} s_k(t)s_{k-1}(t)dt = \begin{cases} E_b \text{ , if} s_k(t) = s_{k-1}(t) \\ -E_b \text{ , if } s_k(t) = -s_{k-1}(t) \end{cases} \tag{1.19}$$

Let $Y_t = \sqrt{\rho}h_t s_t + n_t$; where s_t is the transmitted symbol and n_t is the noise component.

$$\begin{aligned} Y_{t-1}^* Y_t &= (H^* S_{t-1}^* + N_{t-1}^*)(HS_t + N_t) \\ &= |H|^2 S_{t-1}^* S_t + H^* S_{t-1}^* N_t + HS_t N_{t-1}^* + N_t N_{t-1} \\ &= |H|^2 X_t + N, \text{ where } N = H^* S_{t-1}^* N_t + HS_t N_{t-1}^* + N_t N_{t-1} \end{aligned} \tag{1.20}$$

From the above equation, it can be seen that:

$$X_t = \text{sign}(Y_{t-1}^* Y_t) \tag{1.21}$$

Figure 1.30 shows the example of a differential coding when the message sequence $\{a_k\}_{k=0}^{\infty}$ is transmitted. It can be seen that the decoder doesn't depend on the channel fading. In addition, since the noise has two noise terms, it follows that such system is 3 dB worse than the coherent PSK [24].

Modulation	ref.									
Message a_k		1	0	1	1	0	0	0	1	1
Encoding $d_k = \overline{a_k \oplus d_{k-1}}$	1	1	0	0	0	1	0	1	1	1
Signal phase θ	0	0	π	π	π	0	π	0	0	0
Demodulation										
$\frac{l}{E_b} = \frac{1}{E_b}\int_{kT}^{(k+1)T} s_k(t)s_{k-1}(t)dt$		1	-1	1	1	-1	-1	-1	1	1
Demodulator output $\widehat{a}_k$		1	0	1	1	0	0	0	1	1

FIGURE 1.30: example of differential coding

1.3.3.2 Advantages

The main advantage of BPSK is that it doesn't require the knowledge of the channel in order to estimate the transmitted symbol. For high mobility broadband scenarios, estimating the channel becomes very challenging as its parameters become large and hard to track; hence, increasing the complexity and the cost of the system. A convenient solution would be to use incoherent detection. The information in BPSK lies in the phase of two consecutive symbols and it was shown in the previous section the maximum likelihood condition was based on the sign of these two symbols and not the parameters of the fading channel.

1.3.3.3 Limitations

The penalty paid for not knowing the channel's characteristics is a 3 dB signal-to-noise ratio loss compared to coherent detection where the channel's characteristics are perfectly known at the receiver.

1.4 MIMO-UWB

Despite the huge bandwidth and rich diversity due to the abundant multipaths in UWB systems that result in an increase in the channel capacity. Combining such technology with MIMO systems over indoor channels further increases the channel capacity allowing to achieve data rates exceeding 1 Gb/s [38]. This is because MIMO systems allow the increase of spectral efficiency through antenna diversity and array gains. Being a power efficient modulation scheme and because it is very hard to track the amplitude and phase of UWB pulses, these pulses will be modulated in PPM.

The literature of ST coding is huge [19], [21], [25]; however, associating ST codes for IR-UWB is a challenging task. All the known ST coding schemes bring a constellation expansion when associated with PPM. Alamouti code for example introduces $\pm s_i$ or $\pm s_i^*$. It is clear that such encoding scheme is not suitable for PPM without introducing a constellation expansion because $-s_i$ and s_i^* are not part of the PPM constellation codebook. Several attempts tackled this problem and were able to design rate-1 ST codes suitable for PPM which does not require any constellation expansion and provide full diversity order. Coherent system approaches are discussed in [39], [40], [41] and a differential system approach is discussed in [42].

In [39] a binary PPM constellation was adopted where the information symbols are represented by 2-dimensional vectors belonging to the set:

$$C = \left\{ \begin{bmatrix} 1 & 0 \end{bmatrix}^T, \quad \begin{bmatrix} 0 & 1 \end{bmatrix}^T \right\} \tag{1.22}$$

Where the '1' and '0' represent the existence and absence of a UWB pulse respectively. The constructed space-time code is represented by a $2n \times n$ matrix where n is the

number of transmit antennas.

$$C(s_1,\ldots,s_n) = \begin{bmatrix} s_1 & s_2 & \ldots & s_n \\ \Omega s_n & s_1 & \ddots & \vdots \\ \vdots & \ddots & \ddots & s_2 \\ \Omega s_2 & \ldots & \Omega s_n & s_1 \end{bmatrix} \tag{1.23}$$

Where s_1, s_2,..., $s_n \in C$ and Ω stands for the 2×2 cyclic permutation matrix given by:

$$\Omega = \begin{bmatrix} 0 & 1 \\ 1 & 0 \end{bmatrix} \tag{1.24}$$

Since Ωs belongs to C, the proposed code does not provide any constellation extension.

In addition, the full rank property of this rate-1 code allows it to achieve a full transmit diversity order with $n = 2^k$. This can be easily seen as the difference between any two symbols belongs to the following set:

$$\begin{aligned} A &= \{s - s'; s, s' \in C\} \\ &= \left\{ \begin{bmatrix} 0 & 0 \end{bmatrix}^T, \begin{bmatrix} 1 & -1 \end{bmatrix}^T, \begin{bmatrix} -1 & 1 \end{bmatrix}^T \right\} \end{aligned} \tag{1.25}$$

The terms in eq. (1.23) do not belong to any of the codewords in C. From eq. (1.21) it can be observed that this coherent code achieves the rate of 1 symbol per channel use.

In [40], a scheme based on combining PPM and PAM to UWB-IR systems is proposed where a full rate code is achieved having a full transmit diversity order.

The above mentioned implementations assume perfect knowledge of the channel at the receiver. However and since tracking the channel's parameters could be a very difficult task in UWB systems, alternative solutions were provided in the literature. These include the use of autocorrelation receivers instead of Rake receivers that correlate the received signal with a previous one, such system is known as transmitted-reference

signaling (TR) [30] [31] [32], non-coherent solutions are based on energy detection [28] [29] [37] and differential solutions that are based on DPSK [43] [44]. However it is worth mentioning that all of these codes targeted SISO systems.

An interesting approach for noncoherent detection in MIMO-UWB systems is implementing differential schemes. Such schemes are well researched and different ST codes are established for MIMO narrow band systems when the channel is unknown. However, very few contributions targeted implementing differential schemes for IR-UWB MIMO systems [42]. There are many particularities that render the use of existent differential techniques associated with narrow band communications to cope with UWB systems challenging [42]. We describe some of these challenges.

- IR-UWB is carrierless and its pulses are assumed to be real since it is very hard to maintain information on the phase; hence, designing a differential ST code for UWB should satisfy the constraint that it should be real. However in narrow band systems all the differential ST codes are complex-valued; hence not suitable for UWB systems.

- The difference in modulation schemes between both technologies follow. In IR-UWB, PPM is often used due to the temporal fine resolution associated with UWB. However, narrow band communication uses PSK or QAM as a differential modulation scheme which are not compatible with PPM.

- It is very hard to control the amplitude of the UWB low duty cycle pulses. Thus polarity inversions associated with traditional differential systems will be challenging and will render the system more complicated and costly.

In [42], a new differential ST code is proposed for MIMO-UWB systems that doesn't require information of the channel, uses M-PPM modulation scheme with no constellation extension thus shape preserving for all values of M, provides a real differential

ST code and achieves full diversity with any number of transmit antenna P at a normalized code rate of:

$$R = \frac{\log_2(MP)}{P \log_2 M} \tag{1.26}$$

The scheme is based on differential block coding with M-ary PPM constellation where the information symbols belong to the following codebook:

$$C_{ppm} = \{e_m; m = 1, \ldots, M\} \tag{1.27}$$

Where e_m stands for the m$-th$ column of the $M \times M$ identity matrix I_m

The proposed encoding scheme is based on the following rule:

$$S^{(t)} = \mathbf{C_{z_t}} S^{(t-1)} \tag{1.28}$$

Where:

S is the transmitted block at time t and $t-1$ respectively,

z_t is the transmitted data and belongs to $\{0, \ldots, PM-1\}$

$\mathbf{C_{zt}}$ is a $PM \times PM$ matrix,

In [42], a unitary differential space-time construction set C is proposed. This set will include all possible values of $\mathbf{C}$.

$$C = \{\mathbf{C}_i = \mathbf{A}^i | i = 0, \ldots, PM-1\} \tag{1.29}$$

Where:

$$\mathbf{A} = \begin{bmatrix} \mathbf{0_{M\times M}} & \ldots & \mathbf{0_{M\times M}} & \mathbf{\Omega} \\ \mathbf{I_M} & \ldots & \mathbf{0_{M\times M}} & \mathbf{0_{M\times M}} \\ \ldots & \ddots & \vdots & \vdots \\ \mathbf{0_{M\times M}} & \ldots & \mathbf{I_M} & \mathbf{0_{M\times M}} \end{bmatrix} \tag{1.30}$$

And the cyclic permutation $\mathbf{\Omega}$ is given by:

$$\mathbf{\Omega} = \begin{bmatrix} \mathbf{0_{1\times(M-1)}} & 1 \\ \mathbf{I_{(M-1)}} & \mathbf{0_{(M-1)\times 1}} \end{bmatrix} \tag{1.31}$$

And $0_{m\times n}$ is the all-zero $m \times n$ matrix.

At the receiver side, a maximum likelihood (ML) decoder processes the incoming signals under the following rule:

$$\hat{z}_t = \arg \min_{i=0,\ldots,PM-1} \|Y^{(t)} - C_i Y^{(t-1)}\|^2 \tag{1.32}$$

Where $||.||^2$ stands for the Frobenius norm.

1.5 Goal of the Thesis and Provided Work

In this work, we consider a MIMO system for IR-UWB technology with two transmit antennas where the channel is unknown at both the receiver and the transmitter. In systems where it is hard to track the channel's parameters at the receiver due to its highly selective frequency imposed by of the IR-UWB pulses that are spread over a large bandwidth, thus collecting a big number of multipath components is necessary and power consuming, incoherent systems found their way as a motivating solution that are cost and power efficient.

The main goal of this thesis is to provide a noncoherent ST code with unipolar Pulse Position Modulation (PPM) with two transmit. While previous codes require phase rotation or amplitude amplification which are not suitable for PPM modulation without the introduction of a constellation expansion, the proposed scheme avoids all type of amplitude and phase extensions. The 2×2 noncoherent ST code is designed based on a previous coherent code in [41].

1.5.1 A 2x2 Space-Time Code for Noncoherent UWB Communication and Energy Detectors system with M-PPM

Using a PPM modulation scheme, the information signals are transmitted in a specific slot of the PPM window frame. Because of the structure of ST code (2×2), the symbols transmitted will span two time intervals. s_1 and s_2 are transmitted simultaneously by transmitters one and two respectively in the first time interval then in the second time interval Ωs_2 and s_1 are transmitted likewise. The receiver will combine and decode the incoming symbols after evaluating the energies in each of the M slots.

The scheme provided by this work respects the following constraints:

1.5.1.1 Fully Diverse

A full transmit diversity is achieved for all values of M (even number). Increasing the value of M will not affect the slope of the performance curve rather will increase the coding gain. However, this full transmit diversity is obtained at the expense of reduced coding rate given by:

$$R_n = \frac{\log_2 \left(\frac{M(M-2)}{2} \right)}{2} \tag{1.33}$$

This rate is smaller than $\log_2 M$ that is achieved by encoded M-PPM SISO systems. We prove that this is the maximum achievable rate over the constraint of energy detection.

1.5.1.2 Shape Preserving Property

Given the nature of the ST code proposed in [41] and given that the cyclic permutation matrix Ω defines a closed operation on C; where C is the M-ary PPM constellation, the code is shape preserving with PPM where, it is totally equivalent to single antenna

system transmitting only one unipolar pulse in one of the M PPM slots thus rendering the suggested scheme attractive to low-cost IR-UWB systems.

1.5.1.3 Energy Detection

The proposed scheme can be associated with energy detection at the receiver side. In order to eliminate interference between the different modulation positions, the modulation delay δ is taken to be greater than the channel delay spread.

1.5.1.4 Block-by-Block Modulation

Block-by-block modulation is considered in this work. In contrast to differential space-time coding where the symbols reside in the difference between two consecutive signals, the transmitted symbols in block-by-block modulation are independent from each others.

A brief comparison between differential IR-UWB STBC in [42] and the proposed noncoherent space-time block systems is summarized in the following table:

TABLE 1.1: Differential vs Noncoherent STBC for M-PPM

Differential STBC	Noncoherent STBC
No CSI	No CSI
Unipolar signals	Unipolar signals
Shape preserving	Shape preserving
Fully diverse	Fully diverse
For any number of transmit antennas P	For two transmit antennas
Digital decoding	Analog decoding
$R = \frac{\log_2(MP)}{P}$	$R = \frac{\log_2\left(\frac{M(M-2)}{2}\right)}{2}$
Can not be applied with energy detectors	Can be applied with energy detectors

A comparison between the code rates of the differential STBC and the non-coherent STBC shows that for small values of M, $M \leq 6$ for $P = 2$, it is more convenient to apply differential ST code; however, for large values of M, $M > 6$ for $P = 2$, the non-coherent ST code outperforms the differential one. Figure 1.31 compares the code rates of both systems for different values of M and for $P = 2$. Figure 1.32 compares the normalized code rates of these systems where it demonstrates the advantage of our non-coherent system for $M > 6$.

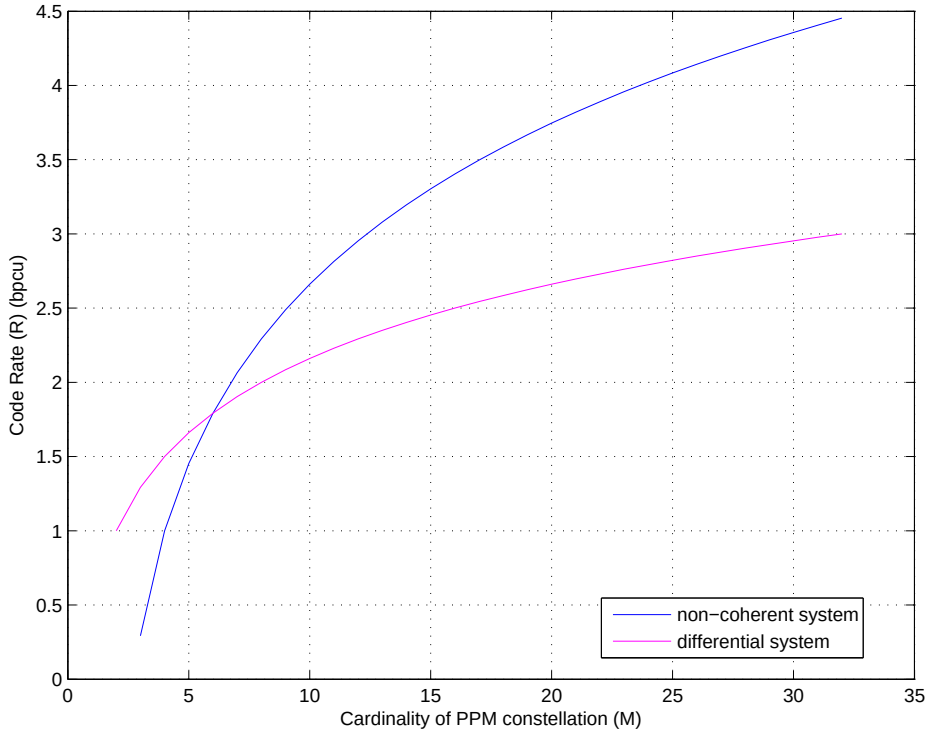

FIGURE 1.31: non-coherent vs differential systems code rates

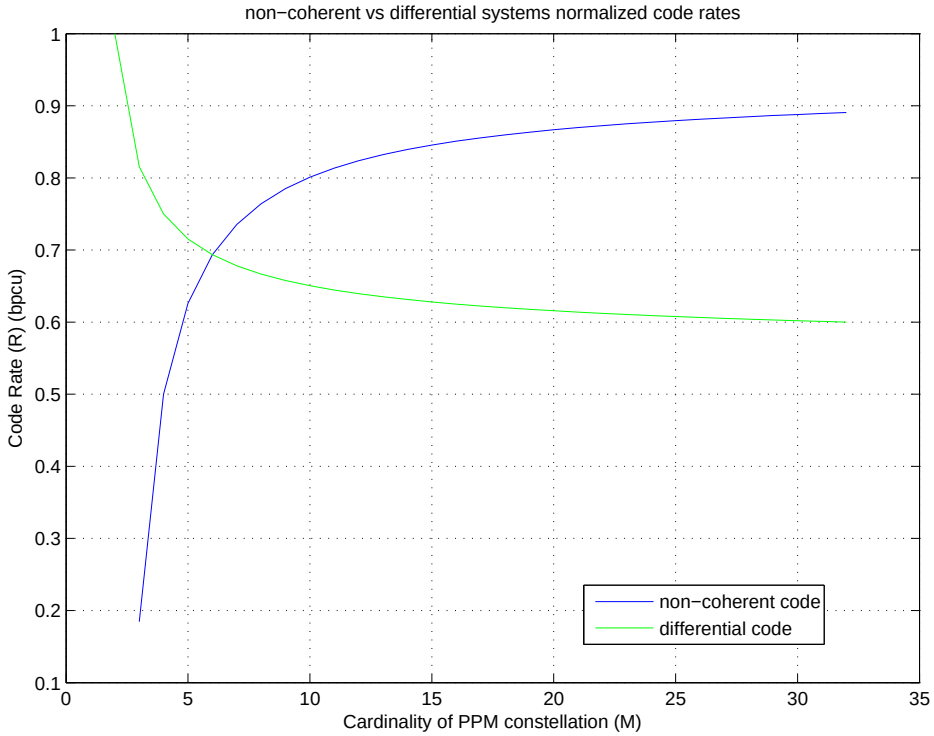

FIGURE 1.32: non-coherent vs differential systems normalized code rates

Chapter 2

PERFORMANCE ANALYSIS

In order to achieve a full transmit diversity order with IR-UWB system with M-PPM modulation scheme, a systematic analysis is performed throughout this chapter. The analysis is based on a previous coherent space-time code block presented in [41] as follows:

$$\begin{bmatrix} s_1 & \Omega s_2 \\ s_2 & s_1 \end{bmatrix} \tag{2.1}$$

Where Ω is a $M \times M$ cyclic permutation matrix described in eq. (1.31).

A system model is first presented followed by a detailed analysis of our work in both SISO and MIMO systems.

2.1 System Model

In this code, the system to be considered is designed to have two transmit and one receive antennas, where in the first time interval the symbols s_1 and s_2 are transmitted by Tx_1 and Tx_2 and in the second time interval the symbols Ωs_2 and s_1 are transmitted by Tx_1 and Tx_2 following the structure of the above STBC in (2.1).

Consider the M-PPM constellation where the information symbols are represented by elements pf the set: $S = \{1, \ldots, M\}$. Let s_p be the symbol transmitted by the p-th antenna in the first time interval having the following structure: $A = \{e_m; m = 1, \ldots, M\}$; where e_m is the m-th column of the $M \times M$ identity matrix. For instance, for $M = 4$, the transmitted symbols have the following structure: s

$$Symbol\ 1 = e_1 = \begin{bmatrix} 1 & 0 & 0 & 0 \end{bmatrix}^T \tag{2.2a}$$

$$Symbol\ 2 = e_2 = \begin{bmatrix} 0 & 1 & 0 & 0 \end{bmatrix}^T \tag{2.2b}$$

$$Symbol\ 3 = e_3 = \begin{bmatrix} 0 & 0 & 1 & 0 \end{bmatrix}^T \tag{2.2c}$$

$$Symbol\ 4 = e_4 = \begin{bmatrix} 0 & 0 & 0 & 1 \end{bmatrix}^T \tag{2.2d}$$

At the receiver side, the decision variables are based on the energy collected in the different M slots of the received signal. We denote by h_1 the impulse response of the channel from the first transmitter ($T\text{x}_1$) and h_2 the impulse response of the channel from the second transmitter ($T\text{x}_2$). The decision variables in the on and off slots can be expressed as follows:

$$y_{on} = H + n_{on} \tag{2.3a}$$

$$y_{off} = n_{off} \tag{2.3b}$$

Where H stands for the energy of the impulse response received in a PPM slot that can take one of the following forms:

$$H_1 = \int_0^{T_i} h_1^2 dt \tag{2.4a}$$

$$H_2 = \int_0^{T_i} h_2^2 dt \tag{2.4b}$$

$$H_{1,2} = \int_0^{T_i} (h_1 + h_2)^2 dt \tag{2.4c}$$

Where:

H_1 is the energy collected when only the first transmitter transmits in a PPM slot.
H_2 is the energy collected when only the second transmitter transmits in a PPM slot.
$H_{1,2}$ is the energy collected when both transmitters transmit simultaneously in the same PPM slot.
T_i is the integration time expressed in seconds.
n_{on} and n_{off} are real white Gaussian noise with zero mean and power $P_{0,\text{on}} = \sigma^2_{\text{on}} = \frac{HN_0T_i}{2}$ and $P_{0,\text{off}} = \sigma^2_{\text{off}} = \frac{N_0T_i}{2}$.

Because our model tackles diversity gain at high SNR, the stand alone squared noise terms (n_i^2) will be ignored, since at high SNR, these terms are negligible.

With coherent systems, the transmitted pair $(s_1, s_2) \in S^2$. It will be proven in this work that a full transmit diversity can be achieved with a non-coherent systems for (s_1, s_2) belonging to a subset C of S^2 which we will derive its maximum size and structure.

2.2 Non-Coherent SISO-IR-UWB System

The model used for simulating IR-UWB signals is based on the SV-model where the incoming rays arrive in clusters. Consider the codebook S of size M given by:

$$S = \{1, \ldots, M\} \tag{2.5}$$

Let s be an $M - PPM$ symbol $\in S$. At the receiver side, an energy collector is used in order to demodulate the incoming symbols. The non-coherent maximum likelihood

decoder (ML) is based on the following rule:

$$\tilde{s} = \arg \max_{i=1,\ldots,M} \{E_i\} \tag{2.6}$$

Where E_i is the energy collected in the i-th PPM slot. Consequently in a non-coherent SISO system, the receiver decides in favor of the symbol that corresponds to the slot having the maximum amount of energy. Since we are transmitting only one symbol in one time interval window T_w, the code rate of the SISO system is given by:

$$R_{SISO} = \frac{\log_2 M}{P} = \frac{\log_2 M}{1} \text{ bits per channel use; where } P \text{ is the number of transmit antennas} \tag{2.7}$$

This rate will be later used in MIMO-IR-UWB systems for normalization.

2.3 Non-Coherent MIMO-IR-UWB System

Consider the STBC in (2.1) and let $(s_1, s_2) \in S^2$ be the transmitted symbols over the channel. These transmitted pairs can be expressed as follows:

$$S^2 = \{(a, b); a, b = 1, \ldots, M\} \tag{2.8}$$

The non-coherent decision variable is based on the maximum likelihood decoder similar to the SISO system having the following rule:

$$(\tilde{s_1}, \tilde{s_2}) = \arg \max_{(s_1,s_2)\in S^2} \{E_{1,s_1} + E_{1,s_2} + E_{2,s_1} + E_{2,\Omega s_2}\} \tag{2.9}$$

Where:

E_{1,s_1} is the energy collected at the receiver from the first transmitter in the first time interval;

E_{1,s_2} is the energy collected at the receiver from the first transmitter in the second time interval;

E_{2,s_1} is the energy collected at the receiver from the second transmitter in the first time interval;

$E_{2,\Omega s_2}$ is the energy collected at the receiver from the second transmitter in the second time interval.

2.3.1 Non-Coherent Detection

Consider the case of 4-PPM and let $(s_1, s_2) = (1, 1)$ be the transmitted symbols as shown in figure 2.1.

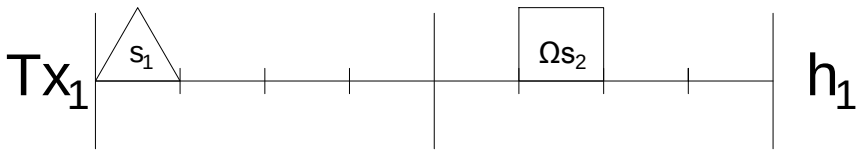

(A) Transmitter 1

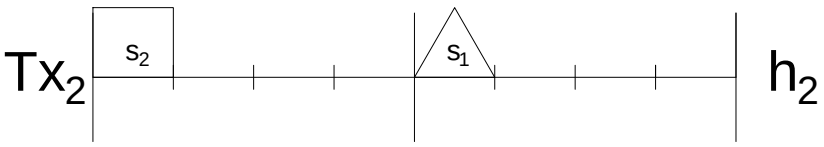

(B) Transmitter 2

FIGURE 2.1: Transmitted symbols over the channel according to the STBC

The energy collected at the receiver in favor of receiving the pair $(1, 1)$ is:

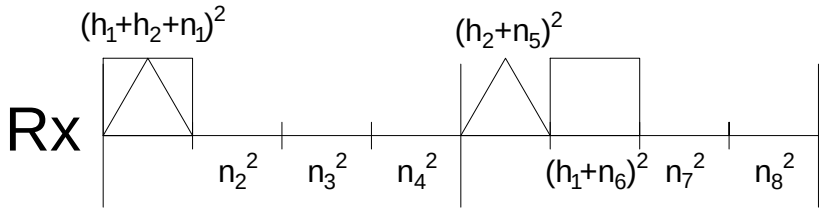

FIGURE 2.2: Receiver

$$\begin{aligned} E &= E_{11} + E_{12} + E_{21} + E_{22} \\ &\triangleq P = (h_1 + h_2 + n_1)^2 + (h_2 + n_5)^2 + (h_1 + n_6)^2 \end{aligned} \tag{2.10}$$

Where n_i is the noise present in the i-th PPM slot. Now we will calculate the probability of error of transmitting $(s_1, s_2) = (1, 1)$ and receiving $(s_1', s_2') \neq (s_1, s_2)$ neglecting the stand alone squared noise quantities in the high SNR regime. We will consider the following three cases:

1. $\mathbf{S'(1, 2)}$: Transmitting symbols (1,1) and deciding in favor of symbols (1,2).

$$S'(1, 2) \triangleq Q = (h_1 + h_2 + n_1)^2 + n_2^2 + (h_2 + n_5)^2 + n_7^2 \tag{2.11}$$

$$
\begin{aligned}
P_e(S'|S) &= \mathrm{P_r}(Q \geq P) \\
&= \mathrm{P_r}((h_1 + h_2 + n_1)^2 + n_2^2 + (h_2 + n_5)^2 + n_7^2 \geq \\
&(h_1 + h_2 + n_1)^2 + (h_2 + n_5)^2 + (h_1 + n_6)^2) \\
&= \mathrm{P_r}(0 \geq (h_1 + n_6)^2) \\
&= \mathrm{P_r}(0 \geq h_1^2 + 2h_1 n_6 + n_6^2) \\
&\simeq \mathrm{P_r}(2h_1 n6 \leq -h_1^2) \\
&= Q\left(\frac{h_1^2}{2\sqrt{h_1^2 N_0}}\right) \\
&= Q\left(\frac{H_1}{2\sqrt{H_1 N_0}}\right)
\end{aligned}
\tag{2.12}
$$

Where $Q(.)$ is the Q function defined as follows:

$$
Q(z) = \frac{1}{\sqrt{2\pi}} \int_z^\infty e^{-\frac{\lambda^2}{2}} d\lambda \tag{2.13}
$$

2. $\mathbf{S'(2,4)}$: Transmitting symbols (1,1) and deciding in favor of symbols (2,4).

$$
S'(2,4) \triangleq Q = n_2^2 + n_4^2 + (h_1 + n_6)^2 + (h_2 + n_5)^2 \tag{2.14}
$$

$$
\begin{aligned}
P_e(S'|S) &= \mathrm{P_r}(Q \geq P) \\
&= \mathrm{P_r}(n_2^2 + n_4^2 + (h_1 + n_6)^2 + (h_2 + n_5)^2 \geq \\
&(h_1 + h_2 + n_1)^2 + (h_2 + n_5)^2 + (h_1 + n_6)^2) \\
&\simeq \mathrm{P_r}(0 \geq (h_1 + h_2 + n_1)^2) \\
&= \mathrm{P_r}(0 \geq (h_1 + h_2)^2 + 2(h_1 + h_2)n_1) \\
&= \mathrm{P_r}(2(h_1 + h_2)n_1 \leq -(h_1 + h_2)^2) \\
&= Q\left(\frac{(h_1 + h_2)^2}{2\sqrt{(h_1 + h_2)^2 N_0}}\right) \\
&= Q\left(\frac{H_{1,2}}{2\sqrt{H_{1,2}N_0}}\right)
\end{aligned}
\tag{2.15}
$$

3. $\mathbf{S'(3,2)}$: Transmitting symbols (1,1) and deciding in favor of symbols (3,2).

$$
S'(3,2) \stackrel{\Delta}{=} Q = n_2^2 + n_3^2 + n_7^2 \tag{2.16}
$$

$$
\begin{aligned}
P_e(S'|S) &= \mathrm{P_r}(Q \geq P) \\
&= \mathrm{P_r}(n_2^2 + n_3^2 + n_7^2 \geq \\
&(h_1 + h_2 + n_1)^2 + (h_2 + n_5)^2 + (h_1 + n_6)^2) \\
&\simeq \mathrm{P_r}(0 \geq (h_1 + h_2 + n_1)^2 + (h_2 + n_5)^2 + (h_1 + n_6)^2) \\
&= \mathrm{P_r}(0 \geq (h_1 + h_2)^2 + 2(h_1 + h_2)n_1 + h_2^2 + 2h_2 n_5 + h_1^2 + 2h_1 n_6) \\
&= \mathrm{P_r}(2(h_1 + h_2)n_1 + 2h_2 n_5 + 2h_1 n_6 \leq -(h_1 + h_2)^2 - h_1^2 - h_2^2) \\
&= Q\left(\frac{(h_1 + h_2)^2 + h_1^2 + h_2^2}{2\sqrt{((h_1 + h_2)^2 + h_1^2 + h_2^2)N_0}}\right) \\
&= Q\left(\frac{H_{1,2} + H_1 + H_2}{2\sqrt{(H_{1,2} + H_1 + H_2)N_0}}\right)
\end{aligned}
\tag{2.17}
$$

Based on the above analysis, we can summarize the pairwise probability of error $P_e(S\prime|S)$ for each pair of symbols as shown in the tables below.

TABLE 2.1: Summary of the pairwise probability of error $P_{e|H}$ (1)

s \ s'	(1,1)	(1,2)	(1,3)	(1,4)
(1,1)	–	$\frac{H_1}{2\sqrt{H_1N_0}}$	$\frac{H_1}{2\sqrt{H_1N_0}}$	$\frac{H_1}{2\sqrt{H_1N_0}}$
(1,2)	$\frac{H_{1,2}}{2\sqrt{H_{1,2}N_0}}$	–	$\frac{H_1+H_2}{2\sqrt{(H_1+H_2)N_0}}$	$\frac{H_1+H_2}{2\sqrt{(H_1+H_2)N_0}}$
(1,3)	$\frac{H_{1,2}}{2\sqrt{H_{1,2}N_0}}$	$\frac{H_1+H_2}{2\sqrt{(H_1+H_2)N_0}}$	–	$\frac{H_1+H_2}{2\sqrt{(H_1+H_2)N_0}}$
(1,4)	$\frac{H_2}{2\sqrt{H_2N_0}}$	$\frac{H_2}{2\sqrt{H_2N_0}}$	$\frac{H_2}{2\sqrt{H_2N_0}}$	–
(2,1)	$\frac{H_{1,2}+H_1}{2\sqrt{(H_{1,2}+H_1)N_0}}$	$\frac{H_{1,2}}{2\sqrt{H_{1,2}N_0}}$	$\frac{H_1+H_{1,2}}{2\sqrt{(H_1+H_{1,2})N_0}}$	$\frac{H_1+H_{1,2}}{2\sqrt{(H_1+H_{1,2})N_0}}$
(2,2)	$\frac{H_1+H_{1,2}}{2\sqrt{(H_1+H_{1,2})N_0}}$	$\frac{H_2}{2\sqrt{H_2N_0}}$	$\frac{H_1+H_2+H_{1,2}}{2\sqrt{(H_1+H_2+H_{1,2})N_0}}$	$\frac{H_1+H_2+H_{1,2}}{2\sqrt{(H_1+H_2+H_{1,2})N_0}}$
(2,3)	$\frac{2H_1+H_2}{2\sqrt{(2H_1+H_2)N_0}}$	$\frac{H_1+2H_2}{2\sqrt{(H_1+2H_2)N_0}}$	$\frac{H_1+H_2}{2\sqrt{(H_1+H_2)N_0}}$	$\frac{2H_1+2H_2}{2\sqrt{(2H_1+2H_2)N_0}}$
(2,4)	$\frac{H_1+H_2}{2\sqrt{(H_1+H_2)N_0}}$	$\frac{2H_2}{2\sqrt{2H_2N_0}}$	$\frac{H_1+2H_2}{2\sqrt{(H_1+2H_2)N_0}}$	$\frac{H_1+H_2}{2\sqrt{(H_1+H_2)N_0}}$
(3,1)	$\frac{H_1+H_2}{2\sqrt{(H_1+H_2)N_0}}$	$\frac{2H_1}{2\sqrt{2H_1N_0}}$	$\frac{H_1+H_2}{2\sqrt{(H_1+H_2)N_0}}$	$\frac{2H_1+H_2}{2\sqrt{(2H_1+H_2)N_0}}$
(3,2)	$\frac{H_1+H_2+H_{1,2}}{2\sqrt{(H_1+H_2+H_{1,2})N_0}}$	$\frac{H_1}{2\sqrt{H_1N_0}}$	$\frac{H_2+H_{1,2}}{2\sqrt{(H_2+H_{1,2})N_0}}$	$\frac{H_1+H_2+H_{1,2}}{2\sqrt{(H_1+H_2+H_{1,2})N_0}}$
(3,3)	$\frac{H_1+H_2+H_{1,2}}{2\sqrt{(H_1+H_2+H_{1,2})N_0}}$	$\frac{H_1+H_{1,2}}{2\sqrt{(H_1+H_{1,2})N_0}}$	$\frac{H_2}{2\sqrt{H_2N_0}}$	$\frac{H_1+H_2+H_{1,2}}{2\sqrt{(H_1+H_2+H_{1,2})N_0}}$
(3,4)	$\frac{H_1+2H_2}{2\sqrt{(H_1+2H_2)N_0}}$	$\frac{H_1+H_2}{2\sqrt{(H_1+H_2)N_0}}$	$\frac{2H_2}{2\sqrt{2H_2N_0}}$	$\frac{H_1+H_2}{2\sqrt{(H_1+H_2)N_0}}$
(4,1)	$\frac{H_1+H_2}{2\sqrt{(H_1+H_2)N_0}}$	$\frac{2H_1+H_2}{2\sqrt{(2H_1+H_2)N_0}}$	$\frac{2H_1}{2\sqrt{2H_1N_0}}$	$\frac{2H_1+H_2}{2\sqrt{(2H_1+H_2)N_0}}$
(4,2)	$\frac{2H_1+2H_2}{2\sqrt{(2H_1+2H_2)N_0}}$	$\frac{H_1+H_2}{2\sqrt{(H_1+H_2)N_0}}$	$\frac{2H_1+H_2}{2\sqrt{(2H_1+H_2)N_0}}$	$\frac{H_1+2H_2}{2\sqrt{(H_1+2H_2)N_0}}$
(4,3)	$\frac{H_1+H_2+H_{1,2}}{2\sqrt{(H_1+H_2+H_{1,2})N_0}}$	$\frac{H_1+H_2+H_{1,2}}{2\sqrt{(H_1+H_2+H_{1,2})N_0}}$	$\frac{H_1}{2\sqrt{H_1N_0}}$	$\frac{H_2+H_{1,2}}{2\sqrt{(H_2+H_{1,2})N_0}}$
(4,4)	$\frac{H_2+H_{1,2}}{2\sqrt{(H_2+H_{1,2})N_0}}$	$\frac{H_2+H_{1,2}}{2\sqrt{(H_2+H_{1,2})N_0}}$	$\frac{H_{1,2}}{2\sqrt{H_{1,2}N_0}}$	$\frac{H_2}{2\sqrt{H_2N_0}}$

TABLE 2.2: Summary of the pairwise probability of error $P_{e|H}$ (2)

s \ s'	(2,1)	(2,2)	(2,3)	(2,4)
(1,1)	$\frac{H_2}{2\sqrt{H_2N_0}}$	$\frac{H_2+H_{1,2}}{2\sqrt{(H_2+H_{1,2})N_0}}$	$\frac{H_2+H_{1,2}}{2\sqrt{(H_2+H_{1,2})N_0}}$	$\frac{H_{1,2}}{2\sqrt{H_{1,2}N_0}}$
(1,2)	$\frac{H_1+H_2}{2\sqrt{(H_1+H_2)N_0}}$	$\frac{H_1+H_2}{2\sqrt{(H_1+H_2)N_0}}$	$\frac{2H_1+H_2}{2\sqrt{(2H_1+H_2)N_0}}$	$\frac{2H_1}{2\sqrt{2H_1N_0}}$
(1,3)	$\frac{H_1+2H_2}{2\sqrt{(H_1+2H_2)N_0}}$	$\frac{2H_1+2H_2}{2\sqrt{(2H_1+2H_2)N_0}}$	$\frac{H_1+H_2}{2\sqrt{(H_1+H_2)N_0}}$	$\frac{2H_1+H_2}{2\sqrt{(2H_1+H_2)N_0}}$
(1,4)	$\frac{H_2+H_{1,2}}{2\sqrt{(H_2+H_{1,2})N_0}}$	$\frac{H_1+H_2+H_{1,2}}{2\sqrt{(H_1+H_2+H_{1,2})N_0}}$	$\frac{H_1+H_2+H_{1,2}}{2\sqrt{(H_1+H_2+H_{1,2})N_0}}$	$\frac{H_1}{2\sqrt{H_1N_0}}$
(2,1)	–	$\frac{H_2}{2\sqrt{H_2N_0}}$	$\frac{H_2}{2\sqrt{H_2N_0}}$	$\frac{H_2}{2\sqrt{H_2N_0}}$
(2,2)	$\frac{H_2}{2\sqrt{H_2N_0}}$	–	$\frac{H_1}{2\sqrt{H_1N_0}}$	$\frac{H_1+H_2}{2\sqrt{(H_1+H_2)N_0}}$
(2,3)	$\frac{H_1+H_2}{2\sqrt{(H_1+H_2)N_0}}$	$\frac{H_1+H_2}{2\sqrt{(H_1+H_2)N_0}}$	–	$\frac{H_1+H_2}{2\sqrt{(H_1+H_2)N_0}}$
(2,4)	$\frac{H_1+H_2}{2\sqrt{(H_1+H_2)N_0}}$	$\frac{H_1+H_2}{2\sqrt{(H_1+H_2)N_0}}$	$\frac{H_1+H_2}{2\sqrt{(H_1+H_2)N_0}}$	–
(3,1)	$\frac{H_1+H_2}{2\sqrt{(H_1+H_2)N_0}}$	$\frac{H_1+H_2}{2\sqrt{(H_1+H_2)N_0}}$	$\frac{2H_2}{2\sqrt{2H_2N_0}}$	$\frac{H_1+2H_2}{2\sqrt{(H_1+2H_2)N_0}}$
(3,2)	$\frac{H_1+H_{1,2}}{2\sqrt{(H_1+H_{1,2})N_0}}$	$\frac{H_1}{2\sqrt{H_1N_0}}$	$\frac{H_{1,2}}{2\sqrt{H_{1,2}N_0}}$	$\frac{H_1+H_{1,2}}{2\sqrt{(H_1+H_{1,2})N_0}}$
(3,3)	$\frac{H_1+H_2+H_{1,2}}{2\sqrt{(H_1+H_2+H_{1,2})N_0}}$	$\frac{H_1+H_{1,2}}{2\sqrt{(H_1+H_{1,2})N_0}}$	$\frac{H_2}{2\sqrt{H_2N_0}}$	$\frac{H_1+H_2+H_{1,2}}{2\sqrt{(H_1+H_2+H_{1,2})N_0}}$
(3,4)	$\frac{2H_1+2H_2}{2\sqrt{(2H_1+2H_2)N_0}}$	$\frac{2H_1+H_2}{2\sqrt{(2H_1+H_2)N_0}}$	$\frac{H_1+2H_2}{2\sqrt{(H_1+2H_2)N_0}}$	$\frac{H_1+H_2}{2\sqrt{(H_1+H_2)N_0}}$
(4,1)	$\frac{2H_1+H_2}{2\sqrt{(2H_1+H_2)N_0}}$	$\frac{H_1+2H_2}{2\sqrt{(H_1+2H_2)N_0}}$	$\frac{H_1+H_2}{2\sqrt{(H_1+H_2)N_0}}$	$\frac{H_2}{2\sqrt{H_2N_0}}$
(4,2)	$\frac{2H_1+2H_2}{2\sqrt{(2H_1+2H_2)N_0}}$	$\frac{H_1+H_2}{2\sqrt{(H_1+H_2)N_0}}$	$\frac{2H_1}{2\sqrt{2H_1N_0}}$	$\frac{H_1+H_2}{2\sqrt{(H_1+H_2)N_0}}$
(4,3)	$\frac{H_1+H_2+H_{1,2}}{2\sqrt{(H_1+H_2+H_{1,2})N_0}}$	$\frac{H_1+H_2+H_{1,2}}{2\sqrt{(H_1+H_2+H_{1,2})N_0}}$	$\frac{H_1}{2\sqrt{H_1N_0}}$	$\frac{H_2+H_{1,2}}{2\sqrt{(H_2+H_{1,2})N_0}}$
(4,4)	$\frac{H_1+H_2+H_{1,2}}{2\sqrt{(H_1+H_2+H_{1,2})N_0}}$	$\frac{H_1+H_2+H_{1,2}}{2\sqrt{(H_1+H_2+H_{1,2})N_0}}$	$\frac{H_1+H_{1,2}}{2\sqrt{(H_1+H_{1,2})N_0}}$	$\frac{H_2}{2\sqrt{H_2N_0}}$

TABLE 2.3: Summary of the pairwise probability of error $P_{e|H}$ (3)

s \ s'	(3,1)	(3,2)	(3,3)	(3,4)
(1,1)	$\frac{H_2}{2\sqrt{H_2N_0}}$	$\frac{H_1+H_2+H_{1,2}}{2\sqrt{(H_1+H_2+H_{1,2})N_0}}$	$\frac{H_1+H_2+H_{1,2}}{2\sqrt{(H_1+H_2+H_{1,2})N_0}}$	$\frac{H_1+H_{1,2}}{2\sqrt{(H_1+H_{1,2})N_0}}$
(1,2)	$\frac{2H_2}{2\sqrt{2H_2N_0}}$	$\frac{H_1+H_2}{2\sqrt{(H_1+H_2)N_0}}$	$\frac{H_1+2H_2}{2\sqrt{(H_1+2H_2)N_0}}$	$\frac{H_1+H_2}{2\sqrt{(H_1+H_2)N_0}}$
(1,3)	$\frac{H_1+H_2}{2\sqrt{(H_1+H_2)N_0}}$	$\frac{2H_1+H_2}{2\sqrt{(2H_1+H_2)N_0}}$	$\frac{H_1+H_2}{2\sqrt{(H_1+H_2)N_0}}$	$\frac{2H_1}{2\sqrt{2H_1N_0}}$
(1,4)	$\frac{H_2+H_{1,2}}{2\sqrt{(H_2+H_{1,2})N_0}}$	$\frac{H_1+H_2+H_{1,2}}{2\sqrt{(H_1+H_2+H_{1,2})N_0}}$	$\frac{H_1+H_2+H_{1,2}}{2\sqrt{(H_1+H_2+H_{1,2})N_0}}$	$\frac{H_1}{2\sqrt{H_1N_0}}$
(2,1)	$\frac{H_1}{2\sqrt{H_1N_0}}$	$\frac{H_2+H_{1,2}}{2\sqrt{(H_2+H_{1,2})N_0}}$	$\frac{H_1+H_2+H_{1,2}}{2\sqrt{(H_1+H_2+H_{1,2})N_0}}$	$\frac{H_1+H_2+H_{1,2}}{2\sqrt{(H_1+H_2+H_{1,2})N_0}}$
(2,2)	$\frac{H_{1,2}}{2\sqrt{H_{1,2}N_0}}$	$\frac{H_2}{2\sqrt{H_2N_0}}$	$\frac{H_2+H_{1,2}}{2\sqrt{(H_2+H_{1,2})N_0}}$	$\frac{H_2+H_{1,2}}{2\sqrt{(H_2+H_{1,2})N_0}}$
(2,3)	$\frac{2H_1}{2\sqrt{2H_1N_0}}$	$\frac{H_1+H_2}{2\sqrt{(H_1+H_2)N_0}}$	$\frac{H_1+H_2}{2\sqrt{(H_1+H_2)N_0}}$	$\frac{2H_1+H_2}{2\sqrt{(2H_1+H_2)N_0}}$
(2,4)	$\frac{2H_1+H_2}{2\sqrt{(2H_1+H_2)N_0}}$	$\frac{H_1+2H_2}{2\sqrt{(H_1+2H_2)N_0}}$	$\frac{H_1+H_2}{2\sqrt{(H_1+H_2)N_0}}$	$\frac{H_1+H_2}{2\sqrt{(H_1+H_2)N_0}}$
(3,1)	–	$\frac{H_1+H_2}{2\sqrt{(H_1+H_2)N_0}}$	$\frac{H_1+H_2}{2\sqrt{(H_1+H_2)N_0}}$	$\frac{H_1+H_2}{2\sqrt{(H_1+H_2)N_0}}$
(3,2)	$\frac{H_2}{2\sqrt{H_2N_0}}$	–	$\frac{H_2}{2\sqrt{H_2N_0}}$	$\frac{H_2}{2\sqrt{H_2N_0}}$
(3,3)	$\frac{H_1}{2\sqrt{H_1N_0}}$	$\frac{H_1}{2\sqrt{H_1N_0}}$	–	$\frac{H_1}{2\sqrt{H_1N_0}}$
(3,4)	$\frac{H_1+H_2}{2\sqrt{(H_1+H_2)N_0}}$	$\frac{H_1+H_2}{2\sqrt{(H_1+H_2)N_0}}$	$\frac{H_1+H_2}{2\sqrt{(H_1+H_2)N_0}}$	–
(4,1)	$\frac{H_1+H_2}{2\sqrt{(H_1+H_2)N_0}}$	$\frac{2H_1+2H_2}{2\sqrt{(2H_1+2H_2)N_0}}$	$\frac{2H_1+H_2}{2\sqrt{(2H_1+H_2)N_0}}$	$\frac{H_1+2H_2}{2\sqrt{(H_1+2H_2)N_0}}$
(4,2)	$\frac{2H_1+H_2}{2\sqrt{(2H_1+H_2)N_0}}$	$\frac{H_1+H_2}{2\sqrt{(H_1+H_2)N_0}}$	$\frac{H_1+H_2}{2\sqrt{(H_1+H_2)N_0}}$	$\frac{2H_2}{2\sqrt{2H_2N_0}}$
(4,3)	$\frac{H_1+H_{1,2}}{2\sqrt{(H_1+H_{1,2})N_0}}$	$\frac{H_1+H_{1,2}}{2\sqrt{(H_1+H_{1,2})N_0}}$	$\frac{H_1}{2\sqrt{H_1N_0}}$	$\frac{H_{1,2}}{2\sqrt{H_{1,2}N_0}}$
(4,4)	$\frac{H_1+H_2+H_{1,2}}{2\sqrt{(H_1+H_2+H_{1,2})N_0}}$	$\frac{H_1+H_2+H_{1,2}}{2\sqrt{(H_1+H_2+H_{1,2})N_0}}$	$\frac{H_1+H_{1,2}}{2\sqrt{(H_1+H_{1,2})N_0}}$	$\frac{H_2}{2\sqrt{H_2N_0}}$

TABLE 2.4: Summary of the pairwise probability of error $P_{e|H}$ (4)

s \ s'	(4,1)	(4,2)	(4,3)	(4,4)
(1,1)	$\frac{H_2}{2\sqrt{H_2N_0}}$	$\frac{H_1+H_2+H_{1,2}}{2\sqrt{(H_1+H_2+H_{1,2})N_0}}$	$\frac{H_1+H_2+H_{1,2}}{2\sqrt{(H_1+H_2+H_{1,2})N_0}}$	$\frac{H_1+H_{1,2}}{2\sqrt{(H_1+H_{1,2})N_0}}$
(1,2)	$\frac{H_1+2H_2}{2\sqrt{(H_1+2H_2)N_0}}$	$\frac{H_1+H_2}{2\sqrt{(H_1+H_2)N_0}}$	$\frac{H_1+H_2}{2\sqrt{(H_1+H_2)N_0}}$	$\frac{2H_1+H_2}{2\sqrt{(2H_1+H_2)N_0}}$
(1,3)	$\frac{2H_2}{2\sqrt{2H_2N_0}}$	$\frac{H_1+2H_2}{2\sqrt{(H_1+2H_2)N_0}}$	$\frac{H_1+H_2}{2\sqrt{(H_1+H_2)N_0}}$	$\frac{H_1+H_2}{2\sqrt{(H_1+H_2)N_0}}$
(1,4)	$\frac{H_{1,2}}{2\sqrt{H_{1,2}N_0}}$	$\frac{H_1+H_{1,2}}{2\sqrt{(H_1+H_{1,2})N_0}}$	$\frac{H_1+H_{1,2}}{2\sqrt{(H_1+H_{1,2})N_0}}$	$\frac{H_1}{2\sqrt{H_1N_0}}$
(2,1)	$\frac{H_1}{2\sqrt{H_1N_0}}$	$\frac{H_2+H_{1,2}}{2\sqrt{(H_2+H_{1,2})N_0}}$	$\frac{H_1+H_2+H_{1,2}}{2\sqrt{(H_1+H_2+H_{1,2})N_0}}$	$\frac{H_1+H_2+H_{1,2}}{2\sqrt{(H_1+H_2+H_{1,2})N_0}}$
(2,2)	$\frac{H_1+H_{1,2}}{2\sqrt{(H_1+H_{1,2})N_0}}$	$\frac{H_2}{2\sqrt{H_2N_0}}$	$\frac{H_1+H_2+H_{1,2}}{2\sqrt{(H_1+H_2+H_{1,2})N_0}}$	$\frac{H_1+H_2+H_{1,2}}{2\sqrt{(H_1+H_2+H_{1,2})N_0}}$
(2,3)	$\frac{H_1+2H_2}{2\sqrt{(H_1+2H_2)N_0}}$	$\frac{2H_2}{2\sqrt{2H_2N_0}}$	$\frac{H_1+H_2}{2\sqrt{(H_1+H_2)N_0}}$	$\frac{H_1+2H_2}{2\sqrt{(H_1+2H_2)N_0}}$
(2,4)	$\frac{2H_1}{2\sqrt{2H_1N_0}}$	$\frac{H_1+H_2}{2\sqrt{(H_1+H_2)N_0}}$	$\frac{2H_1+H_2}{2\sqrt{(2H_1+H_2)N_0}}$	$\frac{H_1+H_2}{2\sqrt{(H_1+H_2)N_0}}$
(3,1)	$\frac{H_1+H_2}{2\sqrt{(H_1+H_2)N_0}}$	$\frac{2H_1+H_2}{2\sqrt{(2H_1+H_2)N_0}}$	$\frac{H_1+2H_2}{2\sqrt{(H_1+2H_2)N_0}}$	$\frac{2H_1+2H_2}{2\sqrt{(2H_1+2H_2)N_0}}$
(3,2)	$\frac{H_1+H_2+H_{1,2}}{2\sqrt{(H_1+H_2+H_{1,2})N_0}}$	$\frac{H_1}{2\sqrt{H_1N_0}}$	$\frac{H_2+H_{1,2}}{2\sqrt{(H_2+H_{1,2})N_0}}$	$\frac{H_1+H_2+H_{1,2}}{2\sqrt{(H_1+H_2+H_{1,2})N_0}}$
(3,3)	$\frac{H_2+H_{1,2}}{2\sqrt{(H_2+H_{1,2})N_0}}$	$\frac{H_{1,2}}{2\sqrt{H_{1,2}N_0}}$	$\frac{H_2}{2\sqrt{H_2N_0}}$	$\frac{H_2+H_{1,2}}{2\sqrt{(H_2+H_{1,2})N_0}}$
(3,4)	$\frac{2H_1+H_2}{2\sqrt{(2H_1+H_2)N_0}}$	$\frac{2H_1}{2\sqrt{2H_1N_0}}$	$\frac{H_1+H_2}{2\sqrt{(H_1+H_2)N_0}}$	$\frac{H_1+H_2}{2\sqrt{(H_1+H_2)N_0}}$
(4,1)	–	$\frac{H_1+H_2}{2\sqrt{(H_1+H_2)N_0}}$	$\frac{H_1+H_2}{2\sqrt{(H_1+H_2)N_0}}$	$\frac{H_1+H_2}{2\sqrt{(H_1+H_2)N_0}}$
(4,2)	$\frac{H_1+H_2}{2\sqrt{(H_1+H_2)N_0}}$	–	$\frac{H_1+H_2}{2\sqrt{(H_1+H_2)N_0}}$	$\frac{H_1+H_2}{2\sqrt{(H_1+H_2)N_0}}$
(4,3)	$\frac{H_2}{2\sqrt{H_2N_0}}$	$\frac{H_2}{2\sqrt{H_2N_0}}$	–	$\frac{H_2}{2\sqrt{H_2N_0}}$
(4,4)	$\frac{H_1}{2\sqrt{H_1N_0}}$	$\frac{H_1}{2\sqrt{H_1N_0}}$	$\frac{H_1}{2\sqrt{H_1N_0}}$	–

Following the analysis done in (2.10)-(2.17) and the results summarized in the above tables, we can express the probability of transmitting symbols (s_1, s_2) and deciding in favor of (s_1', s_2') at the receiver side as follows:

$$P_{e|H}(S'|S) \triangleq Q\left(\frac{iH_1 + jH_2 + kH_{1,2}}{2\sqrt{(iH_1 + jH_2 + kH_{1,2})N_0}}\right) \tag{2.18}$$

Where this probability is conditioned on the channel state H and i, j, k are positive integers.

2.3.2 Building The Subset of S^2

We will now define the structure of the subset C of the constellation S^2 that suits the ST code in eq. (2.1) and is based on the results obtained in section 2.3.1.

1. **General Observation:** Given the pairs (s_1, s_2) and (s_1', s_2') and eq. (2.18), setting $k = 0$ for $i \neq 0$ and $j \neq 0$ results in a probability of error that scales asymptotically with the squared probability of error for the case of SISO system; hence, a transmit diversity gain can be achieved.

   Proof: For $k = 0$, equation (2.18) can be written as follows:

   $$P_{e|h} \triangleq Q\left(\frac{\sqrt{ih_1^2 + jh_2^2}}{4N_0}\right) \tag{2.19}$$

   Following Chernoff bound: $Q(x) \leq \frac{1}{2}e^{\frac{-x^2}{2}}$, (2.19) can be re-written as:

   $$P_{e|h} \leq \frac{1}{2}e^{-\frac{ih_1^2 + jh_2^2}{4N_0}} \tag{2.20}$$

   Averaging eq. (2.20) over the channel states, we get the following P_e:

   $$\begin{aligned} P_e &= \int_{-\infty}^{+\infty}\int_{-\infty}^{+\infty} P_{e|h}p(h_1)p(h_2)d(h_1)d(h_2) \\ &= \int_{-\infty}^{+\infty}\int_{-\infty}^{+\infty} \frac{1}{2}e^{-\frac{ih_1^2 + jh_2^2}{4N_0}}p(h_1)p(h_2)dh_1dh_2 \end{aligned} \tag{2.21}$$

Where:

$p(h_1)$ is the pdf of the channel impulse response from Tx_1.

$p(h_2)$ is the pdf of the channel impulse response from Tx_2.

Because the channel states h_1 and h_2 are independent and identically distributed (iid), eq. (2.21) can be written as follows:

$$\begin{aligned} P_e &= \frac{1}{2}\int_{-\infty}^{+\infty} e^{-\frac{ih_1^2}{4N_0}} p(h_1)d(h_1) \times \int_{-\infty}^{+\infty} e^{-\frac{jh_2^2}{4N_0}} p(h_2)d(h_2) \\ &= \frac{1}{2}P_{SISO} \times P_{SISO} \\ &= \frac{1}{2}P_{SISO}^2 \end{aligned} \tag{2.22}$$

Where P_{SISO} is the probability of error of the SISO system.

Thus for $k = 0$ and for $i, j > 0$, the pairwise probability of error of transmitting (s_1, s_2) and deciding in favor of another pair (s_1', s_2') results in an increase in the transmit diversity with respect to the SISO system. It is worth mentioning that if $i = 0$ or $j = 0$, the transmit diversity of our model will be equivalent to that of a SISO system.

2. **First Restriction:** This follows from setting $k = 0$; hence, eliminating the parameter $H_{1,2}$. Having $H_{1,2}$ in eq. (2.18) implies that both transmitters are transmitting in the same PPM slot simultaneously; hence, at the receiver, we will have overlapping symbols as shown in figures 2.1, therefore in order to overcome this case and based on the STBC discussed above, the conditions below should be respected:

$$s_1 \neq s_2 \text{ and } \Omega s_1 \neq s_2 \tag{2.23}$$

Following the conditions in (2.21), the set S^2 will be reduced to have a maximum cardinality of $M(M-2)$ where M stands for the maximum number of slots in an M-ary PPM modulation scheme. The table below summarizes the results following the first restriction and taking only the numerator part.

TABLE 2.5: Summary following first restriction

s \ s'	(1,2)	(1,3)	(2,3)	(2,4)	(3,1)	(3,4)	(4,1)	(4,2)
(1,2)	$-$	H_1+H_2	$2H_1+H_2$	$2H_1$	$2H_2$	H_1+H_2	H_1+2H_2	H_1+H_2
(1,3)	H_1+H_2	$-$	H_1+H_2	$2H_1+H_2$	H_1+H_2	$2H_1$	$2H_2$	H_1+2H_2
(2,3)	H_1+2H_2	H_1+H_2	$-$	H_1+H_2	$2H_1$	$2H_1+H_2$	H_1+H_2	$2H_2$
(2,4)	$2H_2$	H_1+2H_2	H_1+H_2	$-$	$2H_1+H_2$	H_1+H_2	$2H_1$	H_1+H_2
(3,1)	$2H_1$	H_1+H_2	$2H_2$	H_1+2H_2	$-$	H_1+H_2	H_1+H_2	$2H_1+H_2$
(3,4)	H_1+H_2	$2H_2$	H_1+2H_2	H_1+H_2	H_1+H_2	$-$	$2H_1+H_2$	$2H_1$
(4,1)	$2H_1+H_2$	$2H_1$	H_1+H_2	$2H_2$	H_1+H_2	H_1+2H_2	$-$	H_1+H_2
(4,2)	H_1+H_2	$2H_1+H_2$	$2H_1$	H_1+H_2	H_1+2H_2	$2H_2$	H_1+H_2	$-$

Note that (iH_1+jH_2) corresponds to $Q\left(\frac{iH_1+jH_2}{2\sqrt{(iH_1+jH_2)N_0}}\right)$

3. **Second Restriction:** In order to achieve a full transmit diversity, both H_1 and H_2 must be present in (2.18); hence, $i \neq 0$ and $j \neq 0$ for $k = 0$. Denote by $E_1((s_1', s_2'))$ and $E_2((s_1', s_2'))$ the energies collected in the first and second symbol durations respectively. The ML decoder compares the energy of the received signal, $E_1 + E_2$, with the energies corresponding to the different codewords available in the codebook C and decides in favor of the codeword having the maximum energy. Let C be the codebook following from the *first restriction*; hence, having a maximum size of $M(M-2)$. Let (s_1, s_2) and $(s_1', s_2') \in C$ be the transmitted and received pairs of symbols respectively. The pairwise probability of errors for $i = 0$ and $j = 0$ based on (2.18) are $P_{e|H} = Q\left(\frac{jH_2}{\sqrt{jH_2N_0}}\right)$ and $P_{e|H} = Q\left(\frac{jH_1}{\sqrt{jH_1N_0}}\right)$ respectively. It will be shown that for any pair (s_1, s_2), there exist two pairs that will result in setting either i or j to zero as shown in table 2.5; hence resulting in a diversity gain deficiency. We will denote these pairs by conjugate 1 and conjugate 2 and will be expressed as follows $(s_1, s_2)^*$ and $(s_1, s_2)^{**}$ where:

$$(s_1, s_2)^* = (\Omega s_2, s_1) \text{ and } (s_1, s_2)^{**} = (s_2, \Omega^{-1} s_1) \tag{2.24}$$

The proof is provided in Appendix A.

Following the two restrictions above, the codebook C subset of S^2 that will result in a full diversity gain will have the following structure:

$$C = \{(s_1, s_2) | s_1 \neq s_2 \text{ ,} \Omega s_1 \neq s_2 \text{ ,} (s_1, s_2)^* \notin C \text{ and } (s_1, s_2)^{**} \notin C\} \tag{2.25}$$

4. **Illustrative Example:** In order to demonstrate the above restrictions, an example will be illustrated for the case of $M = 4$. Let (s_1, s_2) be the pairs $\in S^2$ having the structure $A = e_m; m = 1, \ldots, M$ as explained in section 2.1 and as shown in figure 2.3.

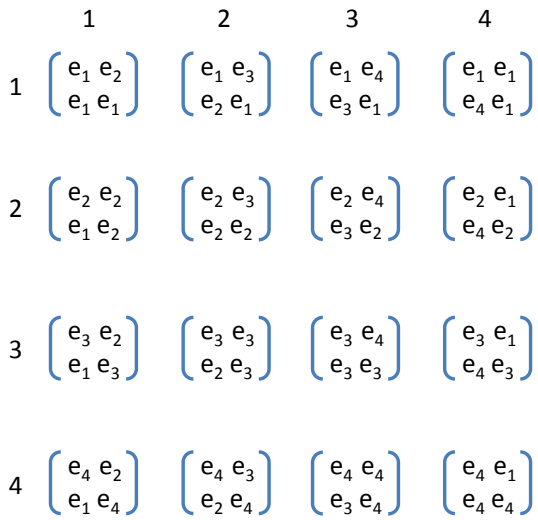

FIGURE 2.3: All S^2 pair of symbols for $M = 4$

In order to satisfy the first restriction, we need to eliminate the pairs that result in having both transmitters transmitting in the same PPM slot; hence, having interference. Following this restriction and based on eq. 2.21, $2M$ pairs will be eliminated as shown in figure 2.4.

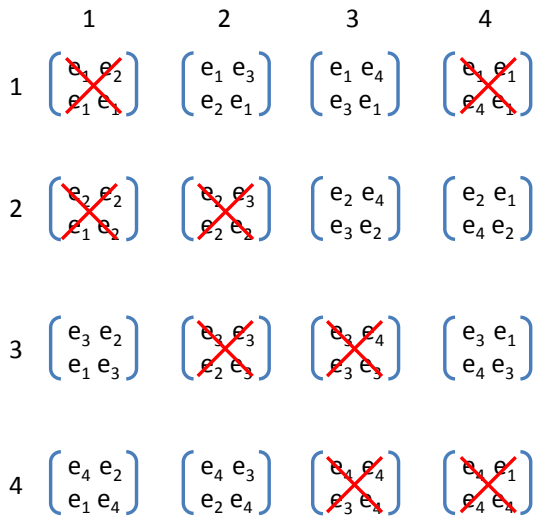

FIGURE 2.4: The remaining codebook after satisfying restriction 1

The second restriction suggests that for each of the remaining pairs, there exist 2 pairs, known as the conjugates, that will result in a non diversity gain; hence, we don't need them to be in our codebook. Figure 2.5 illustrates the conjugates for each of the remaining pair, where the continuous and dashed arrows correspond to the first and second conjugates respectively.

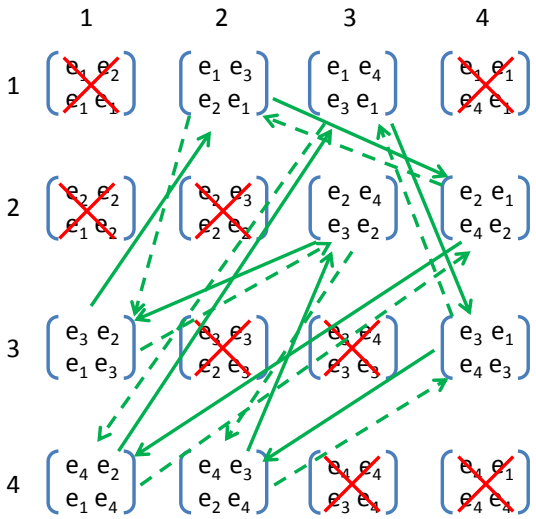

FIGURE 2.5: Illustration based on restriction 2

From figure 2.5, we need to select the maximum number of pairs where neither the first nor the second conjugate of any of the selected pairs are included in the codebook. As a result, there exist two sets of codebooks that satisfy this condition and hence provide a full transmit diversity. Figure 2.6 depicts these codebooks and are as follows:

$$\begin{aligned} C_1 &= [(1,2),(2,3),(3,4),(4,1)] \\ C_2 &= [(1,3),(2,4),(3,1),(4,2)] \end{aligned} \tag{2.26}$$

Where the pairs in C_2 are the conjugates of the pairs in C_1.

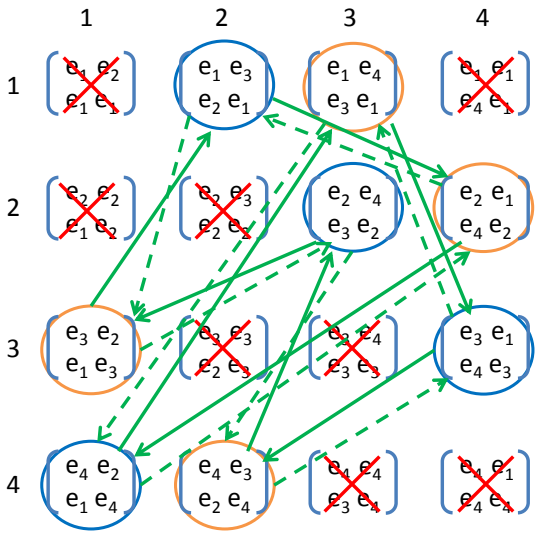

FIGURE 2.6: C_1 and C_2 based on restrictions 1 and 2

2.3.3 Analyzing The Structure of The Set C

Proposition 1: The maximum possible cardinality of the codebook C is $|C| = M\left(\frac{M-2}{2}\right)$.

Proof: We will prove this by contradiction. Let C be the set of distinct pairs of symbols and $\bar{C}$ be the constellation having the conjugate elements of C. Based on equations (2.23) and (2.24), $|C| + |\bar{C}| \leq M(M-2)$. And every element in C (s_1, s_2) admits two distinct conjugates $(s_1, s_2)^*$ and $(s_1, s_2)^{**}$. Assume that $|C| > |\bar{C}|$, in this case some elements in C will share either the first, the second or both conjugates in $\bar{C}$ as shown in figure 2.7, where the blue and green lines correspond to the first and second conjugate respectively. But since the cyclic permutation $\Omega(.)$ and its inverse $\Omega^{-1}(.)$ are bijection functions, if there exist two elements in C sharing the same first or second conjugate in $\bar{C}$ then these elements are identical; hence, contradicting the fact that C admits the set of distinct elements. This will follow that $|C| \leq |\bar{C}|$. Combining this inequality with $|C| + |\bar{C}| \leq M(M-2)$ completes the proof.

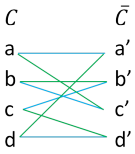

(A) $|C| = |\bar{C}|$

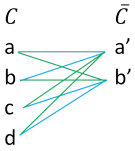

(B) $|C| > |\bar{C}|$

FIGURE 2.7: two cases showing the elements in C and their conjugates in $\bar{C}$

Proposition 2: The structure of the codebook C is: $C = \{\Omega^m(1,n);\ m = 0,\dots M-1,\ n = 2\dots\frac{M}{2}\}$.

Proof: In order to prove the above proposition, it is sufficient to prove that the conjugates of $\{(s_1,s_2) \in C\} \notin C$. Let (s_1,s_2) be the pair of symbols $\in C$: $(s_1,s_2) = \Omega^m(1,n)$, $(s_1,s_2)^* \triangleq (\Omega s_2, s_1) = (\Omega^{m+1}n, \Omega^m 1)$ and $(s_1,s_2)^{**} \triangleq (s_2, \Omega^{-1}s_1) = (\Omega^m n, \Omega^{m-1}1)$. if $(s_1,s_2)^* = (\Omega^{m+1}n, \Omega^m 1) \in C$, then:

$$\begin{aligned} &\Omega^{m+1}n = \Omega^m 1 \\ &\Omega^m 1 = \Omega^m n \\ &\Rightarrow \Omega^{m+1}n = \Omega^m n \end{aligned} \tag{2.27}$$

However from eq. (2.21), $s_1 \neq s_2$, thus the last expression in (2.27) cannot hold; hence, the first conjugate $(s_1,s_2)^* \notin C$. In the same way, if $(s_1,s_2)^{**} = (\Omega^m n, \Omega^{m-1}1) \in C$, then:

$$\begin{aligned} &\Omega^m n = \Omega^m 1 \\ &\Omega^{m-1}1 = \Omega^m n \\ &\Rightarrow \Omega^{m-1}1 = \Omega^m 1 \end{aligned} \tag{2.28}$$

However from eq. (2.21), $\Omega s_1 \neq s_2$, thus the last expression in (2.28) cannot also hold which results in the second conjugate $(s_1, s_2)^{**} \notin C$.

Alternative proof: We will prove that the conjugates of $\{(s_1, s_2) \in C\} \notin C$ in an alternative way. Since $\Omega^{-1}1 = M$, the first conjugate $(s_1, s_2)^* = (\Omega s_2, s_1)$ can be written as: $(s_1, s_2)^* = \Omega^{m+1}(n, M)$ and the second conjugate $(s_1, s_2)^{**} = (s_2, \Omega^{-1}s_1)$ can be written as: $(s_1, s_2)^{**} = \Omega^m(n, M)$. The conjugates therefore belong to the following union set:

$$\begin{aligned}\bar{C} &= \{\Omega^{m+1}(n, M)\}_{m=0}^{M-1} \bigcup \{\Omega^m(n, M)\}_{m=0}^{M-1} \\ &= \{\Omega^m(n, M)\}_{m=1}^{M-1} \bigcup \{\Omega^m(n, M)\}_{m=0}^{M-1} \\ &= \{\Omega^m(n, M)\}_{m=0}^{M-1}\end{aligned} \tag{2.29}$$

Lemma 1: The subset S_0 of S^2 that satisfies eq. (2.21) can be written as:

$$S_0 = \left\{\Omega^m(1, n), \Omega^m(n, M);\ m = 0 \dots M-1,\ n = 2 \dots \frac{M}{2}\right\} \tag{2.30}$$

Where $C = \Omega^m(1, n)$ and $\bar{C} = \Omega^m(n, M)$.

Proof: It can be observed that the set S^2 can be written as:

$$S^2 = \{\Omega^m(1, n);\ m = 0 \dots M-1,\ n = 1 \dots M\} \tag{2.31}$$

From eq. (2.21), $s_1 \neq s_2$ and $s_1 \neq \Omega s_2$. In order to satisfy these conditions, the subset S_0 will become:

$$\begin{aligned}S_0 &= \{\Omega^m(1, n);\ m = 0 \dots M-1,\ n = 2 \dots M-1\} \\ &= \left\{\Omega^m(1, n);\ n = 2 \dots \frac{M}{2}\right\} \bigcup \left\{\Omega^m(1, n);\ n = \frac{M}{2} \dots M-1\right\} \\ &\triangleq S_0^{(1)} \bigcup S_0^{(2)}\end{aligned} \tag{2.32}$$

Where $S_0^{(1)}$ will be our codebook and $S_0^{(2)}$ will be the codebook corresponding to the conjugates.

Performing the change of variable in $S_0^{(2)}$ by setting $n \longrightarrow M - n + 1$, S_0 will be rewritten as:

$$S_0 = \left\{ \Omega^m(1,n);\ n = 2 \dots \frac{M}{2} \right\} \bigcup \left\{ \Omega^m(1, M-n+1);\ n = 2 \dots \frac{M}{2} \right\} \tag{2.33}$$

Setting $\Omega^m(1)$ to $\Omega^m(n)$, $\Omega^m(M-n+1)$ will become:

$$\begin{aligned} \Omega^m(M-n+1) &= \Omega^m(M-n) + \Omega^m(1) \\ &= \Omega^m(M-n) + \Omega^m(n) \\ &= \Omega^m(M-n+n) \\ &= \Omega^m(M) \end{aligned} \tag{2.34}$$

Hence,

$$\begin{aligned} S_0 &= \left\{ \Omega^m(1,n);\ n = 2 \dots \frac{M}{2} \right\} \bigcup \left\{ \Omega^m(n,M);\ n = 2 \dots \frac{M}{2} \right\} \\ &= \left\{ \Omega^m(1,n), \Omega^m(n,M);\ m = 0 \dots M-1,\ n = 2 \dots \frac{M}{2} \right\} \end{aligned} \tag{2.35}$$

Combining equations (2.29) with (2.35) proves the structure of C.

Chapter 3

SIMULATIONS AND RESULTS

In this section, we present the results of some simulations that show the variation of the symbol error rate (SER) as a function of the signal-to-noise ratio (SNR) per information bit. The UWB channels were generated according to the IEEE 802.15.3a NLOS channel model recommendation CM2 for $T_i = 1$ ns and $T_i = 10$ ns respectively.

Figure 3.1 shows the performance with 4-PPM and $T_i = 10$ ns. We compare the numerical results of the proposed system taking the optimal constellation of cardinality $|C| = \frac{M(M-2)}{2}$ (resulting in a full diversity gain), the $M(M-2)$ constellation disregarding restriction 2 explained in section 2.3.2, the M^2 constellation disregarding restrictions 1 and 2 and comparing them with the M constellation of the SISO systems. Results show that the diversity gain of our system taking the optimal constellation outperforms the case of the SISO systems. Whereas disregarding restriction 2 and allowing for the conjugates to coexist in the constellation results in a diversity gain equivalent to the SISO systems as explained in section 2.3.2 and this can be seen by the curve being parallel to the one of the latter at high SNR. However disregarding both restrictions shows a poor performance which is consistent in our analysis since not only we have both conjugates in our constellation but also the pairs that result in having symbols transmitted in the same PPM slot from both transmitters; hence, introducing interference.

Figure 3.2 shows the performance with different values of M for $T_i = 10$ ns and comparing our model with the SISO systems. The results clearly show the improved diversity gain over the SISO systems for all values of M.

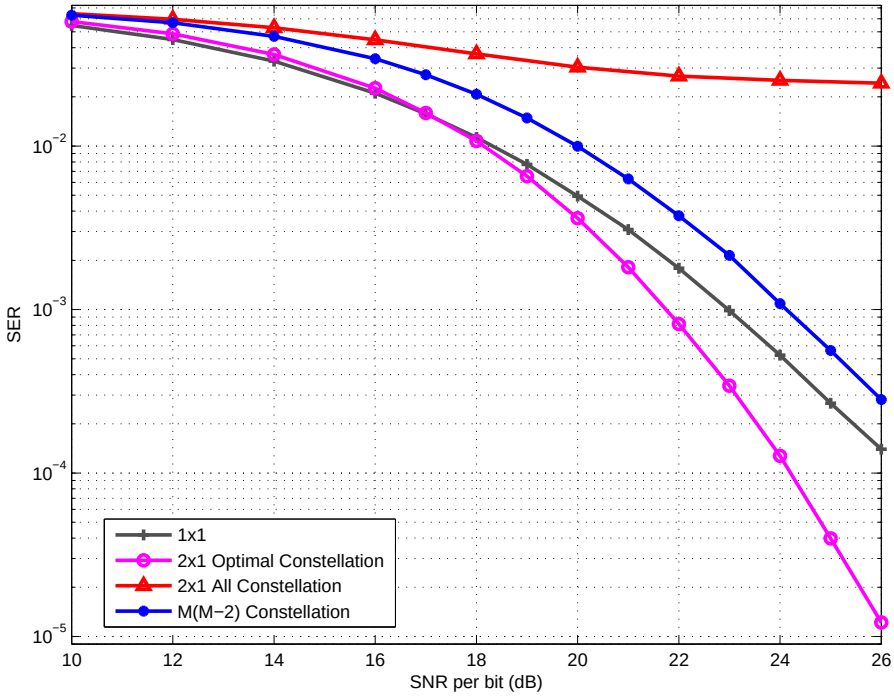

FIGURE 3.1: Performance with 4-PPM and $T_i = 10$ ns

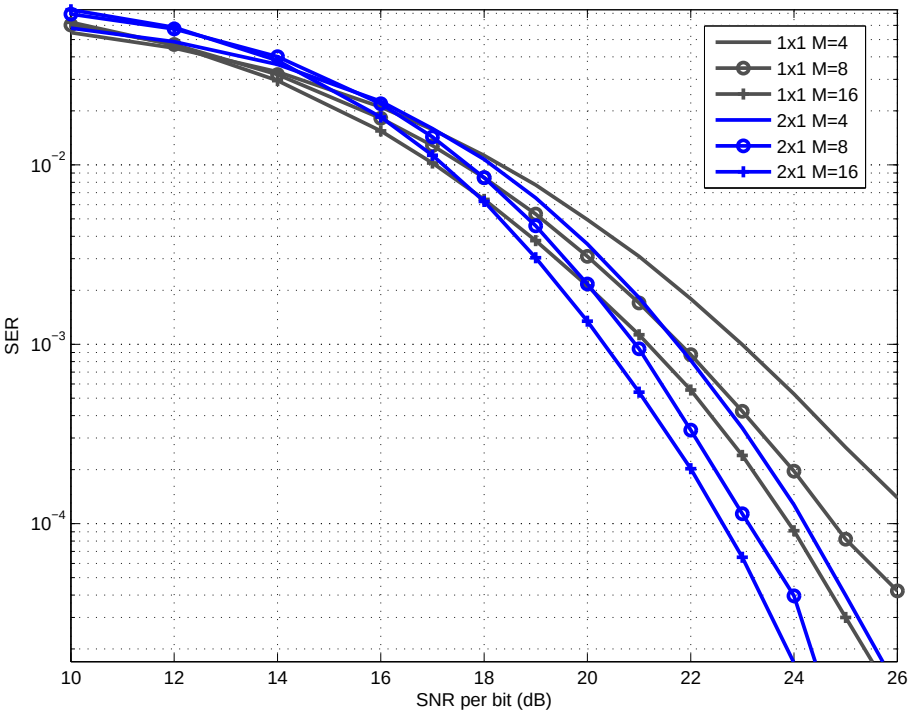

FIGURE 3.2: Performance with M-PPM and $T_i = 10$ ns

Figure 3.3 shows the performance for 6-PPM $T_i = 1$ ns of our system and comparing it with the SISO systems. As for the case of $M = 4$ our system outperforms the SISO systems; however, decreasing the time window T_i shows a degradation in the performance of the system.

Figure 3.4 shows the performance for different values of M where $T_i = 10$ ns of our system comparing two models: A 2x1 and 2x2 systems. Results show an obvious improvement in the performance of the system of around 4 dB.

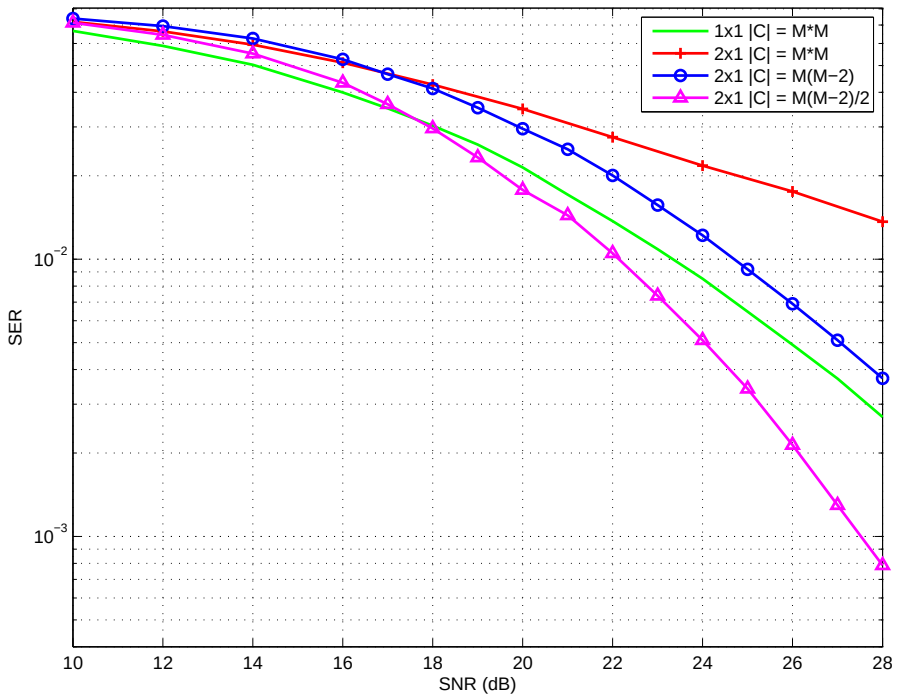

FIGURE 3.3: Performance with 6-PPM and $T_i = 1$ ns

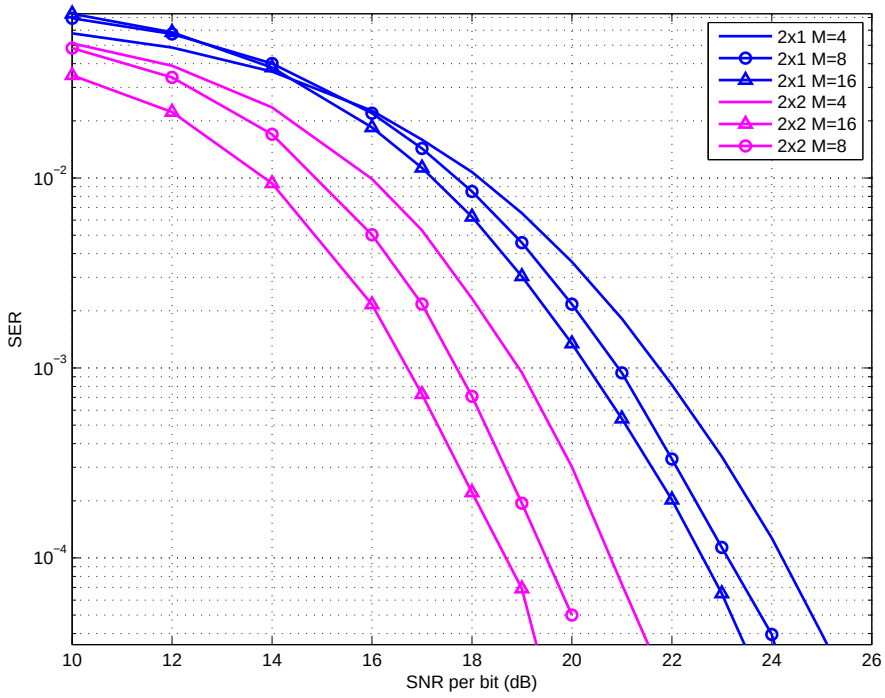

FIGURE 3.4: Performance with M-PPM, $R_x = 2$ and $T_i = 10$ ns

Chapter 4

CONCLUSION and FUTURE WORK

The main topic of this thesis is to combat fading channels for indoor wireless communication systems with UWB technology and non-coherent systems; hence, enhancing the reliability of the communication link. While indoor wireless communication channels exhibit a rich multipath environment, we introduced the concept of space time block code to mitigate the effect of deep fade channels by offering a transmit diversity gain.

On the other hand and because of the power restriction set on UWB signals by the FCC, M-PPM was used to modulate such pulses as it is known to be one of the most power efficient modulation schemes taking advantage of their high temporal resolution.

In this work we have proposed a fully diverse system with IR-UWB technology that does not require the knowledge of the channel state information at neither the transmitter nor the receiver. The discussed model transmits at a rate of one symbol per channel use (pcu) while the receiver is equipped with analog energy detectors that renders the proposed system's complexity very similar to SISO systems.

The full diversity gain was achieved by reducing the codebook S^2 corresponding to coherent systems by eliminating the codewords that result in a diversity gain deficiency. We have also derived the structure of the codebook C subset of S^2 that respects the constraints discussed and analyzed throughout the previous chapters and specifically in section 2.3.2.

While our design is limited to two transmit antennas under white gaussian shot noise with zero mean, future work must consider extending the model to more than two antennas; hence increasing the order of the diversity gain.

Bibliography

[1] F. Nekoogar, *Ultra-Wideband Communications: Fundamentals and Applications*, English, First. Prentice Hall, 2005, p. 240.

[2] J. Foerster, E. Green, S. Somayazulu, and D. Leeper, "Ultra-wideband technology for short- or medium-range wireless communications", *Intel Technology Journal*, 2001.

[3] FCC, "Notice of proposed rule making, "revision of part 15 of the commission's rules regarding ultrawideband transmission systems"", ET-Docket 98-153, 2002.

[4] M. Santhanam, "Uwb technology and its applications – a survey", Tekniska Hogskolan, 2011.

[5] T.Wong and T.Lok, *Theory of digital communications*, Lecture Notes, University of Florida, 2004.

[6] N. Jindal, "Multi-user communication systems: Capacity, duality, and cooperation", Dissertation, stanford university, 2004.

[7] W. P. Siriwongpairat and K. J. R. Liu, *Ultra-Wideband Communications Systems : Multiband OFDM Approach*, English. Wiley, 2007, 229 pp.

[8] C. Abou-Rjeily, "A 2x2 shape-preserving st code for uwb communications with multipulse ppm", *IEEE Transactions on Wireless Communications*, vol. 10, no. 8, pp. 2402–2406, 2011, ISSN: 1536-1276. DOI: 10.1109/TWC.2011.060711.101038.

[9] B. Wilson, *Analogue Optical Fibre Communications (I E E Telecommunications Series)*, B. Wilson, Ed., ed. by Z. Ghassemlooy, ed. by I. Darwazeh. The Institution of Engineering and Technology, 1995, 336 pp.

[10] D.-S. Shiu and J. M. Kahn, "Differential pulse-position modulation for power-efficient optical communication", *IEEE Transactions on Communications*, vol. 47, no. 8, pp. 1201–1210, 1999, ISSN: 0090-6778. DOI: 10.1109/26.780456.

[11] A. K. Majumdar, Ed., *Free-Space Laser Communications*, 1st ed., ed. by J. C. Ricklin, ed. by editorb. Springer-Verlag New York, 2008, 418 pp.

[12] K. Nikolaidis, "An investigation of an optical multiple pulse", Thesis (Doctoral), University of Huddersfield, 2008. [Online]. Available: http://eprints.hud.ac.uk/id/eprint/6980.

[13] Y. Rahayu, T. A. Rahman, and R. Ngah, "Ultra wideband technology and its applications", English, 2008. DOI: 10.1109/WOCN.2008.4542537.

[14] A. A. M. Saleh and R. Valenzuela, "A statistical model for indoor multipath propagation", *IEEE Journal on Selected Areas in Communications*, vol. 5, no. 2, pp. 128–137, 1987, ISSN: 0733-8716. DOI: 10.1109/JSAC.1987.1146527.

[15] D. P. K. Piratla, "Synchronization in impulse based ultra wideband systems", English, Thesis, Virginia Polytechnic Institute and State University, 2008, 80 pp.

[16] M. P. i. Llisterri, "Impact of channel state informationon the analysis and design ofmulti-antenna communication systems", Thesis (Doctoral), Universitat Politecnina de Catalunya, 2006.

[17] J. R. Foerster, M. Pendergrass, and A. F. Molisch, "A channel model for ultra wideband indoor communication", Mistsubishi Electric Research Laboratories, 2003.

[18] M. Matthaiou, *Mimo systems in wireless networks*, Lecture, Chalmers University of Technology, 2011.

[19] M. Jankiraman, *Space-Time Codes and MIMO Systems*, English. Boston: Artech House, 2004.

[20] K. Su, "Space-time coding: From fundamentals to the future", English, Thesis (Doctoral), University of Cambridge, 2003, 112 pp.

[21] B. S. Santumon.S.D, "Space-time block coding (stbc) for wireless networks", English, *International Journal of Distributed and Parallel Systems (IJDPS)*, vol. 3, no. 4, pp. 183–195, 2012.

[22] S. Sandhu, R. Nabar, D. Gore, and A. Paulraj, "Introduction to space-time codes", Report.

[23] C. Abou-Rjeily and J. C. Belfiore, "A rate-1 2x2 space-time code without any constellation extension for th-uwb communication systems with ppm", in *2007 IEEE 65th Vehicular Technology Conference - VTC2007-Spring*, 2007, pp. 1683–1687. DOI: 10.1109/VETECS.2007.350.

[24] O. H. Abdallah, "On developing distributed differential space-time codes", Thesis, The Islamic University of Gaza, Gaza, 2012.

[25] S. M. Alamouti, "A simple transmit diversity technique for wireless communications", *IEEE Journal on Selected Areas in Communications*, vol. 16, no. 8, pp. 1451–1458, 1998, ISSN: 0733-8716. DOI: 10.1109/49.730453.

[26] A. Wittneben, "Basestation modulation diversity for digital simulcast", in *Vehicular Technology Conference, 1991. Gateway to the Future Technology in Motion., 41st IEEE*, 1991, pp. 848–853. DOI: 10.1109/VETEC.1991.140615.

[27] G. J. Foschini, "Layered space-time architecture for wireless communication in a fading environment when using multi-element antennas", *Bell Labs Technical Journal*, vol. 1, no. 2, pp. 41–59, 1996, ISSN: 1089-7089. DOI: 10.1002/bltj.2015.

[28] A. A. D'Amico, U. Mengali, and E. A. de Reyna, "Energy-detection uwb receivers with multiple energy measurements", *IEEE Transactions on Wireless Communications*, vol. 6, no. 7, pp. 2652–2659, 2007, ISSN: 1536-1276. DOI: 10.1109/TWC.2007.05974.

[29] F. Wang, Z. Tian, and B. M. Sadler, "Weighted energy detection for noncoherent ultra-wideband receiver design", *IEEE Transactions on Wireless Communications*,

vol. 10, no. 2, pp. 710–720, 2011, ISSN: 1536-1276. DOI: 10.1109/TWC.2010.120310.101390.

[30] J. D. Choi and W. E. Stark, "Performance of ultra-wideband communications with suboptimal receivers in multipath channels", *IEEE Journal on Selected Areas in Communications*, vol. 20, no. 9, pp. 1754–1766, 2002, ISSN: 0733-8716. DOI: 10.1109/JSAC.2002.805623.

[31] T. Q. S. Quek and M. Z. Win, "Analysis of uwb transmitted-reference communication systems in dense multipath channels", *IEEE Journal on Selected Areas in Communications*, vol. 23, no. 9, pp. 1863–1874, 2005, ISSN: 0733-8716. DOI: 10.1109/JSAC.2005.853809.

[32] M.-H. Chung and R. A. Scholtz, "Receiver improvement for ultra-wideband transmitted-reference systems", in *Wireless Communications and Networking Conference, 2005 IEEE*, vol. 2, 2005, 746–751 Vol. 2. DOI: 10.1109/WCNC.2005.1424601.

[33] K. M. S. Thotahewa, J.-M. Redouté, and M. R. Yuce, *Ultra Wideband Wireless Body Area Networks*, English. Melbourne, Australia: Springer, 2014.

[34] T. M. Duman and A. Ghrayeb, *Coding for MIMO Communication Systems*, English. Wiley, 2007.

[35] V. K. Garg, *Wireless Communications and Networking*, English. San Francisco: Morgan Kaufmann, 2007.

[36] D. Barras, R. Meyer-Piening, G. von Bueren, W. Hirt, and H. Jaeckel, "A low-power baseband asic for an energy-collection ir-uwb receiver", *IEEE Journal of Solid-State Circuits*, vol. 44, no. 6, pp. 1721–1733, 2009, ISSN: 0018-9200. DOI: 10.1109/JSSC.2009.2020199.

[37] C. Carbonelli and U. Mengali, "M-ppm noncoherent receivers for uwb applications", *IEEE Transactions on Wireless Communications*, vol. 5, no. 8, pp. 2285–2294, 2006, ISSN: 1536-1276. DOI: 10.1109/TWC.2006.1687744.

[38] T. Kaiser, F. Zheng, and E. Dimitrov, "An overview of ultra-wide-band systems with mimo", *Proceedings of the IEEE*, vol. 97, no. 2, pp. 285–312, 2009, ISSN: 0018-9219. DOI: 10.1109/JPROC.2008.2008784.

[39] C. Abou-Rjeily and J. C. Belfiore, "A space-time coded mimo th-uwb transceiver with binary pulse position modulation", *IEEE Communications Letters*, vol. 11, no. 6, pp. 522–524, 2007, ISSN: 1089-7798. DOI: 10.1109/LCOMM.2007.070047.

[40] C. Abou-Rjeily, N. Daniele, and J. C. Belfiore, "An optimal 2x2 space-time code for time-hopping ultra-wideband systems with binary pulse position modulation", in *Wireless Communication Systems, 2006. ISWCS '06. 3rd International Symposium on*, 2006, pp. 456–460. DOI: 10.1109/ISWCS.2006.4362339.

[41] C. Abou-Rjeily and W. Fawaz, "Space-time codes for mimo ultra-wideband communications and mimo free-space optical communications with ppm", *IEEE Journal on Selected Areas in Communications*, vol. 26, no. 6, pp. 938–947, 2008, ISSN: 0733-8716. DOI: 10.1109/JSAC.2008.080810.

[42] C. Abou-Rjeily, "Unitary space-time pulse position modulation for differential unipolar mimo ir-uwb communications", *IEEE Transactions on Wireless Communications*, vol. 14, no. 10, pp. 5602–5615, 2015, ISSN: 1536-1276. DOI: 10.1109/TWC.2015.2440270.

[43] K. Witrisal, G. Leus, M. Pausini, and C. Krall, "Equivalent system model and equalization of differential impulse radio uwb systems", *IEEE Journal on Selected Areas in Communications*, vol. 23, no. 9, pp. 1851–1862, 2005, ISSN: 0733-8716. DOI: 10.1109/JSAC.2005.853876.

[44] Q. Zhou and X. Ma, "Receiver designs for differential uwb systems with multiple access interference", *IEEE Transactions on Communications*, vol. 62, no. 1, pp. 126–134, 2014, ISSN: 0090-6778. DOI: 10.1109/TCOMM.2013.120413.130005.

Appendix A

Conjugates of $(\mathbf{s_1}, \mathbf{s_2})$

Let's define the following entities:

- $E_{1,1}$ the energy received in the first symbol duration containing the term H_1
- $E_{1,2}$ the energy received in the second symbol duration containing the term H_1
- $E_{2,1}$ the energy received in the first symbol duration containing the term H_2
- $E_{2,2}$ the energy received in the second symbol duration containing the term H_2

If $i = 0$, then the received signal contains the term H_1; in other words, $E((s_1', s_2')) = E_1((s_1', s_2')) + E_2((s_1', s_2')) = 2H_1$, where $E_1 = E_{1,1} + E_{1,2}$ and $E_2 = E_{2,1} + E_{2,2}$; hence, $P_{e|H} = Q\left(\frac{jH_2}{2\sqrt{jH_2N_0}}\right)$. From the predefined ST code in (2.1), in the first symbol duration, the symbols s_1 and s_2 are transmitted; hence, if $s_1' = s_1$ or $s_2' = s_1$ then the energy collected in the first symbol duration E_1 will contain the term H_1. Similarly, in the second symbol duration, $\Omega(s_2)$ and s_1 are transmitted; hence, if $s_1' = \Omega(s_2)$ or $s_2' = s_2$ then the energy collected in the second symbol duration E_2 will also contain

the term H_1. These conditions can be grouped as follows:

$$\begin{aligned}
&[(s_1' = s_1) \text{ OR } (s_2' = s_1)] \text{ AND } [(s_1' = \Omega s_2) \text{ OR } (s_2' = s_2)] \\
&\Rightarrow [(s_1' = s_1)\text{AND}(s_1' = \Omega s_2)] \text{ OR } [(s_1' = s_1) \text{ AND } (s_2' = s_2)] \\
&\text{OR } [(s_2' = s_1) \text{ AND } (s_1' = \Omega s_2)] \text{ OR } [(s_2' = s_1) \text{ AND } (s_2' = s_2)]
\end{aligned} \tag{A.1}$$

From eq. 2.22, the first expression suggests that $s_1' = s_1 = \Omega s_2$ which is false since it contradicts with eq. 2.21. The second expression is also false because the probability of error is calculated between two distinct pair of symbols. The fourth expression suggest that $s_1 = s_2 = s_2'$ which is always false since it contradicts with eq. 2.21. The third expression however can result in being TRUE if $s_1' = \Omega(s_2)$ and $s_2' = s_1$. Therefore $i = 0$ iff:

$$(s_1', s_2') = (\Omega s_2, s_1) \tag{A.2}$$

Similarly, $j = 0$ if the received signal contains the term H_2. This can be achieved if either $(s_1' = s_2)$ or $(s_2' = s_1)$ are received in the first symbol duration and if either $(s_1' = s_1)$ or $(\Omega s_2' = s_1)$ are received in the second symbol duration. These conditions will result in the following expression:

$$\begin{aligned}
&[(s_1' = s_2) \text{ OR } (s_2' = s_2)] \text{ AND } [(s_1' = s_1) \text{ OR } (\Omega s_2' = s_1)] \\
&\Rightarrow [(s_1' = s_2) \text{ AND } (s_1' = s_1)] \text{ OR } [(s_1' = s_2) \text{ AND } (\Omega s_2' = s_1)] \\
&\text{OR } [(s_2' = s_2) \text{ AND } (s_1' = s_1)] \text{ OR } [(s_2' = s_2) \text{ AND } (\Omega s_2' = s_1)]
\end{aligned} \tag{A.3}$$

From eq. (2.24), the first expression suggests that $s_1' = s_1 = s_2$ which is always false since it contradicts with eq. (2.21). The third expression is always false since the probability of error is calculated between two distinct pair of symbols. The fourth expression suggests that $s_1 = \Omega s_2'$ and $s_2 = s_2'$ which contradicts with (2.21). Therefore, in order for $j = 0$, $s_1' = s_2$ and $\Omega s_2' = s_1$ must be true so that the boolean expression becomes true. In other words, $j = 0$ iff:

$$(s_1', s_2') = (s_2, \Omega^{-1} s_1) \tag{A.4}$$

Equations (2.21) and (2.22) must be associated with the codebook C in order to achieve a full transmit diversity. And for a given pair of symbols $(s_1, s_2) \in C$, $(\Omega s_2, s_1)$ and $(s_2, \Omega^{-1} s_1)$ will be referred to as the first and second conjugates of (s_1, s_2) respectively.